

# On POD-based Deflation Vectors for DPCG applied to porous media problems.

G. B. Diaz Cortes<sup>1</sup>, C. Vuik<sup>1</sup> and J. D. Jansen<sup>2</sup>

<sup>1</sup>Department of Applied Mathematics, TU Delft

<sup>2</sup>Department of Geoscience & Engineering, TU Delft

August 21, 2017

## Abstract

Simulation of two-phase flow through highly heterogeneous porous media results in large systems of linear equations for the pressure equation, when using e.g., sequential procedures. During simulation, the most time consuming part is the solution of the resulting linear system. In this work, solution of the elliptic pressure equation is studied with preconditioning and deflation techniques based on information obtained from the system.

For a good performance of deflation techniques, it is necessary to find good deflation vectors. If a good selection of these vectors is made, only a small increase in the required computing time per iteration and an important decrease in the number of iterations is achieved.

In this work, we propose the capture of a series of snapshots, solutions of the system with slightly different configuration. A POD-reduced basis obtained from these snapshots is proposed as deflation vectors. We investigate convergence and the properties of the resulting methods. We perform a series of numerical experiments with diverse conditions. We consider incompressible two-phase flow in a layered model with variations in the permeability layers up to  $10^6$  and the SPE 10 benchmark model with a contrast in permeability coefficients of  $10^7$ . We study 2D and 3D reservoirs, taking into account gravity terms for the 3D case. We consider immiscible fluids with and without capillary pressure. We study water flooding, with injection through the boundaries and through wells.

# 1 Introduction

## 1.1 Two phase flow through porous media

When simulating two phase flow through a porous medium, these two phases can be considered as separated, i.e., they are immiscible and there is no mass transfer between them. The contact area between the phases is known as the interface.

When modeling two phases, we usually consider one of the fluids as the wetting phase ( $w$ ), which is more attracted to the mineral particles than the other phase. The other phase is considered as non-wetting phase ( $n$ ). In the case of a water-oil system, water is considered the wetting phase.

The saturation of a phase ( $S_\alpha$ ), is the fraction of void space filled with that phase in the medium, where a zero saturation indicates that the phase is not present. If there are two phases present in the porous medium, these fluids fill completely the empty space, which is expressed by the following relation,

$$S_n + S_w = 1. \quad (1)$$

The surface tension and the curvature of the interface between the fluids causes a difference in pressure between the two phases. This difference is known as the capillary pressure,  $p_c$ , which, depends on the saturation:

$$p_c(S_w) = p_n - p_w. \quad (2)$$

The pressure of the non-wetting fluid is higher than the pressure of the wetting fluid, therefore, the capillary pressure is always a positive quantity. The relation between the capillary pressure and the saturation is obtained as an empirical model based on experiments. The capillary curve depends on the difference in pore-size distributions, porosity and permeability of the medium. To normalize the measured data, it is common to use a function called Leverett J-function, which takes the following form:

$$J_L(S_w) = \frac{P_c}{\sigma \cos \theta} \sqrt{\frac{K}{\phi}}, \quad (3)$$

where  $\sigma$  is the surface tension,  $\phi$  and  $K$  are the permeability and the porosity of the medium and  $\theta$  the contact angle.

Sometimes, the capillary pressure is expressed as an analytical function of the normalized water saturation ( $\hat{S}_w = \frac{S_w - S_w^{min}}{S_w^{max} - S_w^{min}}$ ). A model for the relationship between the capillary pressure and water saturation was proposed by Brooks and Corey (for water and air):

$$\hat{S}_w = \begin{cases} (p_c/p_e)^{-n_b} & \text{if } p_c > p_e \\ 1 & p_c \leq p_e \end{cases}$$

where  $p_e$  is the pressure of air, and  $n_b$  is related to the pore-size distribution. Another model was proposed by Genuchten:

$$\hat{S}_w = (1 + (\beta_g p_c)_g^n)^{-m_g}, \quad (4)$$

where  $\beta_g$  is related to the average size of pores and  $n_g$  and  $m_g$  are related to the pore size distribution.

### **Relative permeability**

When modeling two phases, the permeability of each phase,  $\alpha$ , will be affected by the presence of the other phase, therefore an effective permeability  $K_\alpha$  for each phase has to be used instead of the absolute permeability  $K$ . Due to interfacial tensions, the sum of all the phase permeabilities is less than one, i.e.,

$$\sum_{\alpha} K_{\alpha}^e < K.$$

The saturation dependent relative permeability is defined as:

$$k_{r\alpha}(S_{\alpha}) = K_{\alpha}^e / K.$$

The simplest model possible that relates the relative permeabilities with the saturations is the is Corey model:

$$\begin{aligned} k_{rw} &= (\hat{S}_w)^{n_w} k_w^0, \\ k_{ro} &= (1 - \hat{S}_w)^{n_o} k_o^0. \end{aligned} \tag{5}$$

where  $n_w > 1$ ,  $n_o > 1$  and  $k_{\alpha}^0$  are fitting parameters.

As in the single-phase case, the governing equations for two-phase flow in a porous medium are the mass conservation and Darcy's law. The mass balance equation for a phase  $\alpha$  is given by:

$$\frac{\partial(\phi \rho_{\alpha} S_{\alpha})}{\partial t} + \nabla \cdot (\rho_{\alpha} \mathbf{v}_{\alpha}) = \rho_{\alpha} q_{\alpha}, \tag{6}$$

and Darcy's law reads:

$$\mathbf{v}_{\alpha} = -\frac{k_{r\alpha}}{\mu_{\alpha}} K (\nabla p_{\alpha} - \rho_{\alpha} g \nabla z). \tag{7}$$

Where,  $\rho_{\alpha}$ ,  $\mu_{\alpha}$ ,  $q_{\alpha}$  and  $p_{\alpha}$  are the density, viscosity, sources and pressure of each phase,  $g$  is the gravity constant, and  $z$  is the depth of the reservoir.

To simplify notation, the phase mobilities ( $\lambda_{\alpha}(S_{\alpha}) = K k_{r\alpha}(S_{\alpha}) / \mu_{\alpha}$ ) are introduced. Combining Darcy's law (7), the mass balance equation (6) and using the phase mobilities, the system reads:

$$\frac{\partial(\phi \rho_{\alpha} S_{\alpha})}{\partial t} - \nabla \cdot (\rho_{\alpha} \lambda_{\alpha} (\nabla p_{\alpha} - \rho_{\alpha} g \nabla z)) = \rho_{\alpha} q_{\alpha}. \tag{8}$$

### **Incompressible two-phase flow**

In the case of incompressible flow, the porosity  $\phi$  and the densities  $\rho_{\alpha}$  do not depend on time. Therefore, Equation (8) reduces to:

$$\phi \frac{\partial S_{\alpha}}{\partial t} - \nabla \cdot (\lambda_{\alpha} (\nabla p_{\alpha} - \rho_{\alpha} g \nabla z)) = q_{\alpha}. \tag{9}$$

A common approach to solve this problem is the fractional flow formulation, where the fractional flow function is defined as:

$$f_{\alpha 1} = \frac{\lambda_{\alpha 1}}{\lambda_{\alpha 1} + \lambda_{\alpha 2}},$$

for a two-phase system with phases  $\alpha 1$  and  $\alpha 2$ .

**Fractional flow formulation**

When we have a wetting (w) and a non wetting phase (n), the system of equations for an incompressible problem reads:

$$\begin{aligned}\phi \frac{\partial S_w}{\partial t} + \nabla \cdot \mathbf{v}_w &= \phi \frac{\partial S_w}{\partial t} + \nabla \cdot (\lambda_w (\nabla p_w - \rho_w g \nabla z)) = q_w, \\ \phi \frac{\partial S_n}{\partial t} + \nabla \cdot \mathbf{v}_n &= \phi \frac{\partial S_n}{\partial t} + \nabla \cdot (\lambda_n (\nabla p_n - \rho_n g \nabla z)) = q_n.\end{aligned}\quad (10)$$

To solve this system, we define the total Darcy's velocity as the sum of the velocity in the wetting and non wetting phases:

$$\begin{aligned}\mathbf{v} = \mathbf{v}_w + \mathbf{v}_n &= -\lambda_n \nabla p_n - \lambda_w \nabla p_w + (\lambda_n \rho_n + \lambda_w \rho_w) g \nabla z \\ &= -(\lambda_n + \lambda_w) \nabla p_n + \lambda_w \nabla p_c + (\lambda_n \rho_n + \lambda_w \rho_w) g \nabla z.\end{aligned}\quad (11)$$

If we add the two continuity equations (System (10)) and use the relationship  $S_n + S_w = 1$ , we have:

$$\phi \frac{\partial (S_w + S_n)}{\partial t} + \nabla \cdot (\mathbf{v}_w + \mathbf{v}_n) = \nabla \cdot \mathbf{v} = q, \quad (12)$$

where  $q = q_n + q_w$  is the total source. Defining the total mobility as  $\lambda = \lambda_n + \lambda_w$ , Equation (12) becomes:

$$-\nabla \cdot (\lambda \nabla p_n) = q - \nabla [\lambda_w \nabla p_c + (\lambda_n \rho_n + \lambda_w \rho_w) g \nabla z], \quad (13)$$

which is an equation for the pressure of the non wetting phase. This equation depends on the saturation via the capillarity  $p_c$  and the total mobility  $\lambda$ .

Multiplying each phase velocity by the relative mobility of the other phase and subtracting the result, together with Equation (11), we get:

$$\begin{aligned}\lambda_n \mathbf{v}_w - \lambda_w \mathbf{v}_n &= \lambda \mathbf{v}_w - \lambda_w \mathbf{v} \\ &= \lambda_w \lambda_n [\nabla p_c + (\rho_w - \rho_n) g \nabla z].\end{aligned}$$

Therefore, for  $\mathbf{v}_w$  we have

$$\mathbf{v}_w = \frac{\lambda_w}{\lambda} \mathbf{v} + \frac{\lambda_w \lambda_n}{\lambda} [\nabla p_c + (\rho_w - \rho_n) g \nabla z].$$

Using the velocity computed above, and the fractional flow function,  $f_w = \frac{\lambda_w}{\lambda_w + \lambda_o}$ , the transport Equation (6) for the wetting phase reads:

$$\phi \frac{\partial S_w}{\partial t} + \nabla \cdot [f_w (\mathbf{v} + \lambda_n \Delta \rho g \nabla z)] + \nabla \cdot (f_w \lambda_n \nabla p_c) = q_w, \quad (14)$$

where  $\Delta \rho = \rho_w - \rho_n$ . With this approach, the system is expressed in terms of the pressure of the non wetting phase, Equation (13), and the saturation of the wetting phase, Equation (14). In the pressure equation, the coupling to saturation is present via the phase mobilities and the derivative of the capillary function. For the saturation, we have an indirect coupling with the pressure through the total Darcy velocity.

## 1.2 Numerical methods

### *Sequential solution procedures*

To solve the system described by Equation (13) and Equation (14), various procedures can be used. For this work, we use the sequential procedure, where, the equations are solved separately in consecutive substeps. An unknown is fixed, e.g., the saturation, and the elliptic equation is solved for the pressure. Once the pressure is computed, it is used to compute the total velocity and to solve the parabolic transport equation. If the capillary pressure is zero, the transport equation becomes hyperbolic.

The sequential solution procedure is sometimes referred as IMPES, implicit pressure, explicit saturation.

### *Temporal discretization*

The saturation equation is time dependent. The time discretization can be performed using two schemes: implicit and explicit. In the explicit scheme, the time derivative is approximated using the solutions obtained for the previous time step, the system to solve, reads:

$$\phi \frac{(S_w^{n+1} - S_w^n)}{\Delta t} + \nabla \cdot [f_w(S_w^n)(\mathbf{v}^n + \lambda_n \Delta \rho g \nabla z)] + \nabla \cdot (f_w(S_w^n) \lambda_n(S_w^n) \nabla p_c(S_w^n)) = q_w^{n+1}. \quad (15)$$

For the implicit solution, backward Euler discretization schemes can be used. With this scheme, Equation (14) is:

$$\phi \frac{(S_w^{n+1} - S_w^n)}{\Delta t} + \nabla \cdot [f_w(S_w^{n+1})(\mathbf{v}^n + \lambda_n \Delta \rho g \nabla z)] + \nabla \cdot (f_w(S_w^{n+1}) \lambda_n(S_w^{n+1}) \nabla p_c(S_w^{n+1})) = q_w^n. \quad (16)$$

That can be rewritten as:

$$\begin{aligned} S_w^{n+1} - S_w^n - \frac{\Delta t}{\phi} (q_w - \nabla \cdot [f_w(S_w^{n+1})(\mathbf{v}^n + \lambda_n \Delta \rho g \nabla z)]) \\ + \frac{\Delta t}{\phi} (\nabla \cdot (f_w(S_w^{n+1}) \lambda_n(S_w^{n+1}) \nabla p_c(S_w^{n+1}))) = 0. \end{aligned} \quad (17)$$

If we use the implicit scheme, the resulting system is nonlinear (Equation (17)) and depends on the saturation at time step  $n$  and  $n + 1$ . The nonlinear system can be solved using Newton-Raphson (NR) method. With this method, for the  $(k + 1)$ -th iteration we have:

$$J(S^k) \delta S^{k+1} = -F(S^k, S^n), \quad S^{k+1} = S^k + \delta S^{k+1},$$

where

$$\begin{aligned} F(S^k, S^n) = S_w^k - S_w^n - \frac{\Delta t}{\phi} (q_w - \nabla \cdot [f_w(S_w^k)(\mathbf{v}^n + \lambda_n \Delta \rho g \nabla z)]) \\ + \frac{\Delta t}{\phi} (\nabla \cdot (f_w(S_w^k) \lambda_n(S_w^k) \nabla p_c(S_w^k))), \end{aligned} \quad (18)$$

$J(S^k) = \frac{\partial F(S^k, S^n)}{\partial S^k}$  is the Jacobian matrix, and  $\delta S^{k+1}$  is the NR update at iteration step  $k + 1$ . Therefore, the linear system to solve is:

$$J(S^k)\delta S^{k+1} = b(S^k). \quad (19)$$

where  $b(S^k)$  is the function evaluated at iteration step  $k$ ,  $b(S^k) = -F(S^k, S^n)$ .

### **Spatial discretization**

As mentioned before, for the sequential procedure we need to solve the equation for pressure and later solve the transport equation. For the pressure we have to solve Equation (13). The spatial derivatives are approximated using a finite difference scheme with cell central differences. For a 3D model, taking a mesh with a uniform grid size  $\Delta x$ ,  $\Delta y$ ,  $\Delta z$  where  $(i, j, l)$  is the center of the cell in the position  $i$  in the  $x$  direction,  $j$  in the  $y$  direction, and  $l$  in the  $z$  direction  $(x_i, y_j, z_l)$ , where  $p_{i,j,l} = p(x_i, y_j, z_l)$  is the pressure at this point. For the  $x$  direction, we have (see, e.g., [1–3]):

$$\begin{aligned} \nabla \cdot (\lambda \nabla p) &= \frac{\partial}{\partial x} \left( \lambda \frac{\partial p}{\partial x} \right) = \frac{\Delta}{\Delta x} \left( \lambda \frac{\Delta p}{\Delta x} \right) + \mathcal{O}(\Delta x^2) \\ &= \frac{\lambda_{i+\frac{1}{2},j,l}(p_{i+1,j,l} - p_{i,j,l}) - \lambda_{i-\frac{1}{2},j,l}(p_{i,j,l} - p_{i-1,j,l})}{(\Delta x)^2} + \mathcal{O}(\Delta x^2), \end{aligned}$$

where  $\lambda_{i-\frac{1}{2},j,l}$  is the harmonic average of the mobility for cells  $(i - 1, j, l)$  and  $(i, j, l)$ :

$$\lambda_{i-\frac{1}{2},j,l} = \frac{2}{\frac{1}{\lambda_{i-1,j,l}} + \frac{1}{\lambda_{i,j,l}}}. \quad (20)$$

After discretization, not taking into account capillary pressure and gravity, and defining the *transmissibility* ( $T_{i-\frac{1}{2},j,l}$ ) between grid cells  $(i - 1, j, l)$  and  $(i, j, l)$  as:

$$T_{i-\frac{1}{2},j,l} = \frac{2\Delta y\Delta z}{\mu\Delta x} \lambda_{i-\frac{1}{2},j,l}, \quad (21)$$

we can rewrite Equation (13), together with boundary conditions, as:

$$\mathbf{T}\mathbf{p} = \mathbf{q}, \quad (22)$$

where  $\mathbf{T}$  is known as the transmissibility matrix, that is a sparse matrix with 3 non zero diagonals in 1D, 5 in 2D and 7 in 3D. System (22) is a linear system that can be solved with iterative or direct methods. For the solution of this system, it is necessary to define boundary conditions at all boundaries of the domain. These conditions can be prescribed pressures (Dirichlet conditions), flow rates (Neumann conditions) or a combination of these (Robin conditions).

### **Well model**

In reservoir simulation, a fluid is typically injected or extracted through wells. During

injection and production, the rate of injection or the bottom hole pressure (bhp) of the well is prescribed.

To model the injection or production through the wells, a linear relationship between the bhp and the flow rate in a well can be used. Taking the cell  $(i, j, l)$  that contains a well, the relationship between the pressure inside the well and the pressure of the cell is given by:

$$q_{(i,j,l)} = I_{(i,j,l)}(p_{(i,j,l)} - p_{bh(i,j,l)}), \quad (23)$$

where  $I_{(i,j,l)}$  is the productivity or injectivity index of the well,  $p_{(i,j,l)}$  is the reservoir pressure in the cell containing the well, and  $p_{bh(i,j,l)}$  is a prescribed pressure inside the well.

*Incompressible fluid*

Using the well model in Equation (22) we obtain:

$$\mathbf{T}\mathbf{p} = \mathbf{I}_w(\mathbf{p} - \mathbf{p}_{bh}), \quad (24)$$

where  $\mathbf{I}_w$  is a diagonal matrix containing the productivity or injectivity indices of the wells present in the reservoir. The diagonal elements are zero for cells without wells and have the value of the well index for each cell containing a well.

### 1.3 Iterative solution methods

When simulating two phase flow through a porous medium, after discretization, using the sequential procedure, we obtain a linear system for the pressure. If the system is large, solving it is time consuming, therefore iterative techniques are preferred over direct methods to solve it. The resulting matrix is SPD (Symmetric Positive Definite), therefore we choose Conjugate Gradient (CG) as iterative method to solve it. We accelerate the solution with the Incomplete Cholesky preconditioner. In this work, we study a further acceleration with deflation and POD techniques. In this section, we give a brief overview of the methods.

#### Conjugate Gradient Method

The CG method is a Krylov-subspace method used when the matrix of the linear system is SPD. This method is based in the minimization of the residual in the  $\mathbf{A}$ -norm.

Given a starting solution  $\mathbf{x}^0$  and the residual defined by  $\mathbf{r}^k = \mathbf{b} - \mathbf{A}\mathbf{x}^k$ , we define the Krylov subspace as  $\mathcal{K}_k(\mathbf{A}, \mathbf{r}^0) = \text{span}\{\mathbf{r}^0, \mathbf{A}\mathbf{r}^0, \dots, \mathbf{A}^{k-1}\mathbf{r}^0\}$ . For this space,  $\mathbf{x}^k \in \mathbf{x}^0 + \mathcal{K}_k(\mathbf{A}, \mathbf{r}^0)$  has a minimal error measured in the  $\mathbf{A}$ -norm for all approximations contained in  $\mathbf{x}^0 + \mathcal{K}_k(\mathbf{A}, \mathbf{r}^0)$ . The error of this approximation is bounded by:

$$\|\mathbf{x} - \mathbf{x}^{k+1}\|_{\mathbf{A}} \leq 2\|\mathbf{x} - \mathbf{x}^0\|_{\mathbf{A}} \left( \frac{\sqrt{\kappa_2(\mathbf{A})} - 1}{\sqrt{\kappa_2(\mathbf{A})} + 1} \right)^{k+1}. \quad (25)$$

Hence, the convergence of the method depends on the condition number ( $\kappa_2$ ) of the matrix. The pseudo code for CG is given in Algorithm 2.

<b>Algorithm 2</b> Conjugate Gradient (CG) method, solving $\mathbf{Ax} = \mathbf{b}$ .
---

<p>Give an initial guess <math>\mathbf{x}^0</math>.          Compute <math>\mathbf{r}^0 = \mathbf{b} - \mathbf{Ax}^0</math> and set <math>\mathbf{p}^0 = \mathbf{r}^0</math>.  <b>for</b> <math>k = 0, \dots</math>, until convergence              <math>\alpha^k = \frac{(\mathbf{r}^k, \mathbf{r}^k)}{(\mathbf{Ap}^k, \mathbf{p}^k)}</math>              <math>\mathbf{x}^{k+1} = \mathbf{x}^k + \alpha^k \mathbf{p}^k</math>              <math>\mathbf{r}^{k+1} = \mathbf{r}^k - \alpha^k \mathbf{Ap}^k</math>              <math>\beta^k = \frac{(\mathbf{r}^{k+1}, \mathbf{r}^{k+1})}{(\mathbf{r}^k, \mathbf{r}^k)}</math>              <math>\mathbf{p}^{k+1} = \mathbf{r}^{k+1} + \beta^k \mathbf{p}^k</math>  <b>end</b></p>
--

#### Preconditioning

To accelerate the convergence of a Krylov method, the system can be transformed into another one containing an iteration matrix with a better spectrum, i.e, a smaller condition

---

<sup>1</sup>The condition number  $\kappa_2(\mathbf{A})$  is defined as  $\kappa_2(\mathbf{A}) = \frac{\sqrt{\lambda_{\max}(\mathbf{A}^T \mathbf{A})}}{\sqrt{\lambda_{\min}(\mathbf{A}^T \mathbf{A})}}$ . If  $\mathbf{A}$  is SPD,  $\kappa_2(\mathbf{A}) = \frac{\lambda_{\max}(\mathbf{A})}{\lambda_{\min}(\mathbf{A})}$ .



number. This can be done by multiplying the linear system by a matrix  $\mathbf{M}^{-1}$ .

$$\mathbf{M}^{-1}\mathbf{A}\mathbf{x} = \mathbf{M}^{-1}\mathbf{b}. \quad (26)$$

The new system has the same solution but can provide a substantial reduction of the condition number. For this preconditioned system, the error is bounded by:

$$\|\mathbf{x} - \mathbf{x}^k\|_{\mathbf{A}} \leq 2\|\mathbf{x} - \mathbf{x}^0\|_{\mathbf{A}} \left( \frac{\sqrt{\kappa(\mathbf{M}^{-1}\mathbf{A})} - 1}{\sqrt{\kappa(\mathbf{M}^{-1}\mathbf{A})} + 1} \right)^k. \quad (27)$$

For the CG method, the matrix  $\mathbf{M}$  is chosen as an *SPD* matrix such that  $\kappa(\mathbf{M}^{-1}\mathbf{A}) \leq \kappa(\mathbf{A})$ , and  $\mathbf{M}^{-1}\mathbf{b}$  is cheap to compute.

### Deflation

The deflation method is used to annihilate the effect of extreme eigenvalues hampering the convergence of an iterative method [4]. Given an *SPD* matrix  $\mathbf{A} \in \mathbb{R}^{n \times n}$ , for a given matrix  $\mathbf{Z} \in \mathbb{R}^{n \times m}$  the deflation matrix  $\mathbf{P}$  is defined as follows ([5, 6]):

$$\mathbf{P} = \mathbf{I} - \mathbf{A}\mathbf{Q}, \quad \mathbf{P} \in \mathbb{R}^{n \times n}, \quad \mathbf{Q} \in \mathbb{R}^{n \times n},$$

where

$$\mathbf{Q} = \mathbf{Z}\mathbf{E}^{-1}\mathbf{Z}^T, \quad \mathbf{Z} \in \mathbb{R}^{n \times m}, \quad \mathbf{E} \in \mathbb{R}^{m \times m},$$

with

$$\mathbf{E} = \mathbf{Z}^T\mathbf{A}\mathbf{Z}.$$

The matrix  $\mathbf{E}$  is known as the *Galerkin* or *coarse* matrix. This matrix has to be invertible, to satisfy this condition  $\mathbf{Z}$  has to be a full rank matrix. The full rank matrix  $\mathbf{Z}$  is called the *deflation – subspace* matrix, and its columns are the *deflation* vectors or *projection* vectors.

### Deflated PCG Method

In this work, the solution of the linear system (24) is performed with the deflated CG method. With this method, instead of solving the original system, we solve the deflated system (see Appendix E):

$$\mathbf{P}\mathbf{A}\hat{\mathbf{x}} = \mathbf{P}\mathbf{b}, \quad (28)$$

for the deflated solution  $\hat{\mathbf{x}}$ . This deflated the solution is related to the solution  $\mathbf{x}$  of the original system as (see Appendix E):

$$\mathbf{x} = \mathbf{Q}\mathbf{b} + \mathbf{P}^T\hat{\mathbf{x}}. \quad (29)$$

The deflated linear system can also be preconditioned by an *SPD* matrix  $\mathbf{M}$ . After preconditioning, the deflated preconditioned system to solve with CG is [6]:

$$\tilde{\mathbf{P}}\tilde{\mathbf{A}}\hat{\hat{\mathbf{x}}} = \tilde{\mathbf{P}}\tilde{\mathbf{b}},$$

where:

$$\tilde{\mathbf{A}} = \mathbf{M}^{-\frac{1}{2}} \mathbf{A} \mathbf{M}^{-\frac{1}{2}}, \quad \hat{\mathbf{x}} = \mathbf{M}^{\frac{1}{2}} \tilde{\mathbf{x}}, \quad \tilde{\mathbf{b}} = \mathbf{M}^{-\frac{1}{2}} \mathbf{b}$$

This method is called the Deflated Preconditioned Conjugate Gradient *DPCG* method. In practice  $\mathbf{M}^{-1} \mathbf{P} \mathbf{A} \mathbf{x} = \mathbf{M}^{-1} \mathbf{P} \mathbf{b}$  is computed and the error is bounded by:

$$\|\mathbf{x} - \mathbf{x}^{i+1}\|_{\mathbf{A}} \leq 2 \|\mathbf{x} - \mathbf{x}^0\|_{\mathbf{A}} \left( \frac{\sqrt{\kappa_{eff}(\mathbf{M}^{-1} \mathbf{P} \mathbf{A})} - 1}{\sqrt{\kappa_{eff}(\mathbf{M}^{-1} \mathbf{P} \mathbf{A})} + 1} \right)^{i+1},$$

where  $\kappa_{eff} = \frac{\lambda_{max}(M^{-1}PA)}{\lambda_{min}(M^{-1}PA)}$  is the effective condition number and  $\lambda_{min}(M^{-1}PA)$  is the smallest non-zero eigenvalue of  $M^{-1}PA$ .

### Choices of Deflation Vectors

The deflation method is used to remove the effect of the most unfavorable eigenvalues of  $\mathbf{A}$ . If the matrix  $\mathbf{Z}$  contains eigenvectors corresponding to the unfavorable eigenvalues, the convergence of the iterative method is achieved faster. However, to obtain and to apply the eigenvectors is costly in view of memory and CPU time. Therefore, a good choice of the matrix  $\mathbf{Z}$  that efficiently approximates the eigenvectors is essential for the applicability of the method.

A good choice of the deflation vectors is usually problem-dependent. Available information on the system is, in general, used to obtain these vectors. Most of the techniques used to choose deflation vectors are based on approximating eigenvectors, recycling [7], subdomain deflation vectors [8] or multigrid and multilevel based deflation techniques [6, 9]. A summary of these techniques is given below.

**Recycling Deflation.** A set of search vectors previously used is reused to build the deflation-subspace matrix [7]. The vectors could be, for example,  $q - 1$  solution vectors of the linear system with different right-hand sides or of different time steps. The matrix  $\mathbf{Z}$  containing these solutions is:

$$\mathbf{Z} = [\mathbf{x}^{(1)}, \mathbf{x}^{(2)}, \dots, \mathbf{x}^{(q-1)}].$$

**Subdomain Deflation.** The domain is divided into several subdomains, using domain decomposition techniques or taking into account the properties of the problem. For each subdomain, there is a deflation vector that contains ones for cells in the subdomain and zeros for cells outside [8].

**Multi Grid and Multilevel Deflation.** For the multigrid and multilevel methods, the prolongation and restriction matrices are used to pass from one level or grid to another. These matrices can be used as the deflation-subspace matrices  $\mathbf{Z}$  [6].

## 1.4 Proper Orthogonal Decomposition (POD)

As mentioned before, in this work we want to combine deflation techniques and Proper Orthogonal Decomposition (POD) to reduce the number of iterations necessary to solve the linear system obtained from reservoir simulation in a cheap and automatic way. In this section, we give a brief overview of the POD method.

The POD method is a Model Order Reduction (MOR) method, where a high-order model is projected onto a space spanned by a small set of orthonormal basis vectors. The high dimensional variable  $\mathbf{x} \in \mathbb{R}^n$  is approximated by a linear combination of  $l$  orthonormal basis vectors [10]:

$$\mathbf{x} \approx \sum_{i=1}^l c_i \psi_i, \quad (30)$$

where  $\psi_i \in \mathbb{R}^n$  are the basis vectors and  $c_i$  are their corresponding coefficients. In matrix notation, equation (30) is rewritten as :

$$\mathbf{x} \approx \Psi \mathbf{c},$$

where  $\Psi = [\psi_1 \ \psi_2 \ \dots \ \psi_l]$ ,  $\Psi \in \mathbb{R}^{n \times l}$  is the matrix containing the basis vectors, and  $\mathbf{c} \in \mathbb{R}^l$  is the vector containing the coefficients of the basis vectors.

The basis vectors  $\psi_i$  are computed from a set of 'snapshots'  $\{\mathbf{x}_i\}_{i=1, \dots, m}$ , obtained by simulation or experiments [11]. In POD, the basis vectors  $\{\psi_j\}_{j=1}^l$ , are  $l$  eigenvectors corresponding to the largest eigenvalues  $\{\sigma_j\}_{j=1}^l$  of the data snapshot correlation matrix  $\mathbf{R}$ .

$$\mathbf{R} := \frac{1}{m} \mathbf{X} \mathbf{X}^T \equiv \frac{1}{m} \sum_{i=1}^m \mathbf{x}_i \mathbf{x}_i^T, \quad \mathbf{X} := [\mathbf{x}_1, \mathbf{x}_2, \dots, \mathbf{x}_m], \quad (31)$$

where  $\mathbf{X} \in \mathbb{R}^{n \times m}$  is an SPSD matrix containing the previously obtained snapshots. The  $l$  eigenvectors should contain almost all the variability of the snapshots. Usually, they are chosen as the eigenvectors of the maximal number ( $l$ ) of eigenvalues satisfying [11]:

$$\frac{\sum_{j=1}^l \sigma_j}{\sum_{j=1}^m \sigma_j} \leq \alpha, \quad 0 < \alpha \leq 1, \quad (32)$$

with  $\alpha$  close to 1. The eigenvalues  $\sigma_j$  are ordered from large to small with  $\sigma_1$  the largest eigenvalue of  $\mathbf{R}$ . It is not necessary to compute the eigenvalues from  $\mathbf{X} \mathbf{X}^T$ , but instead, it is possible to compute the eigenvalues of the much smaller matrix  $\mathbf{X}^T \mathbf{X}$  (see Appendix D).

In this study, we normalize the snapshots, so  $\|\mathbf{x}_i\|_2 = 1$ .

## 2 Numerical experiments

### 2.1 Model problems

We model water flooding into a reservoir initially filled with oil. Therefore, the initial saturation is set as one for the oil and zero for the water (see Table 2). The solution of the systems of linear equations, resulting from the discretization of the partial differential equations describing this process, is studied in this work. Sequential solution procedures are used in this work. The transport equation is solved with the Matlab Reservoir Simulation Toolbox (MRST) [12] using implicit schemes. In this work, we focus on the solution of the pressure equation. We propose the use of the Deflated Conjugate Gradient method preconditioned with Incomplete Cholesky (DICCG) method together with POD to solve this problem. We investigate the use of snapshots-based POD vectors as deflation vectors for DICCG. For the first set of experiments, we compute 10 snapshots to obtain the POD basis. In the second set, we run a training simulation changing the bottom hole pressure of the wells. From this system, we obtain the basis that will be used to solve similar problems.

#### *Pressure solver*

The solution of the pressure equation is approximated with the ICCG and DICCG methods. For the DICCG method, it is necessary to select a set of deflation vectors. Snapshots are taken during the first 10 time steps using the ICCG method. These snapshots are used to compute a POD basis. For the first set of experiments, 10 POD basis vectors are used (DICCG<sub>POD<sub>10</sub></sub>), whereas 5 POD basis vectors (DICCG<sub>POD<sub>5</sub></sub>) are used for the second set of experiments (snapshots-based POD deflation vectors). The matrices corresponding to the linear systems  $\mathbf{A}$  and right-hand sides  $\mathbf{b}$  are obtained with MRST [12].

As tolerance or stopping criterium, we use the relative residual, defined as the 2-norm of the residual of the  $k^{th}$  iteration divided by the 2-norm of the right-hand side of the preconditioned system:

$$\frac{||\mathbf{M}^{-1}\mathbf{r}^k||_2}{||\mathbf{M}^{-1}\mathbf{b}||_2} \leq \epsilon.$$

The stopping criterium of the linear solvers is  $\epsilon = 10^{-11}$ .

In the present section, we give a general overview of the experiments that we perform, but the specifications are presented below for each problem separately.

### Heterogeneous permeability layers

The experiments simulate flow through a porous medium with a constant porosity field of 0.2. For the first set of experiments, we study a layered system (see Figure 1). We use 8 layers of the same size, 4 layers with one value of permeability  $\sigma_1$ , followed by a layer with a different permeability value  $\sigma_2$ . The permeability of one set of layers is set to  $\sigma_1 = 1mD$ , the permeability of the other set  $\sigma_2$  is varied. Therefore, the contrast in permeability between the layers ( $\frac{\sigma_2}{\sigma_1} = \sigma_2$ ), depends on the value of  $\sigma_2$ . The permeability  $\sigma_2$  varies from  $\sigma_2 = 1mD$  to  $\sigma_2 = 10^{-3}mD$ . The domain consists of a Cartesian grid of 32 x 32 cells with a length of one meter each cell. For the relative permeability of the fluids,

the Corey model is used. The properties of the fluids are presented in Table 1. No gravity terms and no capillary pressure are taken into account in the first set of experiments. For the second set, capillary pressure is taken into account. The capillary relationship is linear,  $P_c = C(1 - S)$ . The curve is presented in Figure 3. Finally, we perform 3D experiments with 20 x 20 x 20 grid cells and gravity terms included.

Property	Water	Oil	Units
$\mu$	1	10	$cp$
$\rho$	1000	700	$kg/m^3$
$k_r$	$(S_w)^2$	$(1 - S_w)^2$	
$C_p$	$10 * (1 - S)$		bars

Table 1: Fluids properties.

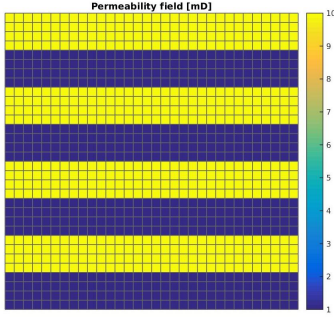


Figure 1: Rock permeability

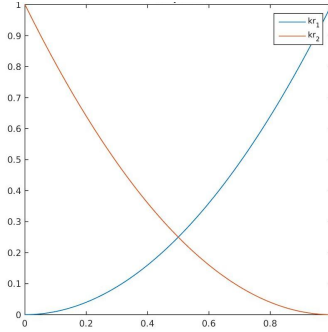


Figure 2: Fluid relative permeability

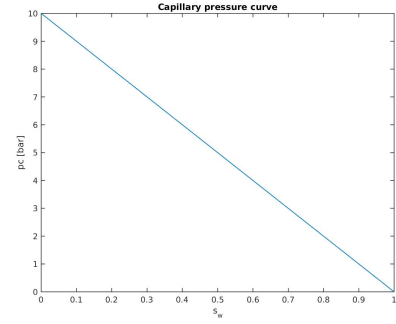


Figure 3: Capillary pressure

### ***Injection through the boundary***

For the first set of experiments, water is injected from one boundary at a rate of  $0.4 m^3/day$  and pressure is set as zero at the right boundary and 100 bars inside the reservoir. Water is injected from the left boundary. The simulation is run during 4800 days with 240 time steps of 20 days (See Table 3).

Initial saturations		
	Water	Oil
$S_{0,x \neq 0, L_x}$	0	1
$S_{x=0}$	1	0
$S_{x=L_x}$	0	1

Table 2: Saturations.

Property	Value	Units
$T_{total}$	4800	days
$T_{steps}$	240	
$dT$	20	days
Boundary conditions		
$Q_{x=0}$	0.4	$m^3/day$
$P_{0,x \neq 0, L_x}$	100	bars
$P_{x=L_x}$	0	bars

Table 3: Initial values of the system.

### Injection through the left boundary, no capillary pressure.

As mentioned before, we simulate flow through a porous media. Water is injected into a reservoir originally filled with oil. Water is injected through the left boundary in an homogeneous reservoir and a layered reservoir. In Table 4, the number of iterations necessary to achieve convergence is presented for various contrast between permeability layers for the deflation method with different selection of deflation vectors. The number of iterations necessary to achieve convergence for the ICCG method is presented in the second column (Total ICCG). The number of iterations necessary to compute the first 10 snapshots with the ICCG method is presented in the 4th column (ICCG Snapshots). In the 5th column, we present the total number of iterations, taking into account the first 10 snapshots computed with ICCG, and the rest of the iterations computed with DICCG. In the last column, the percentage of the total number of iterations of the DICCG methods with respect to the ICCG method is presented.

In Figure 6, the eigenvalues of the correlation matrix are presented. We observe that the last 5 eigenvalues are larger than the rest. Therefore we use as deflation vectors the POD basis created with the eigenvectors corresponding to these five eigenvalues and the basis created with all the snapshots, 10 POD vectors. The pressure field and the water saturation are presented in Figure 4 and Figure 5 for various times.

$\frac{\sigma_2}{\sigma_1}$	Total ICCG	Method	ICCG Snapshots	DICCG	Total ICCG +DICCG	% of total ICCG
$10^0$	12210	DICCG <sub>POD<sub>10</sub></sub>	495	295	790	6
$10^0$	12210	DICCG <sub>POD<sub>5</sub></sub>	495	384	879	7
$10^1$	14783	DICCG <sub>POD<sub>10</sub></sub>	605	1270	1875	13
$10^1$	14783	DICCG <sub>POD<sub>5</sub></sub>	605	1573	2178	15
$10^2$	14513	DICCG <sub>POD<sub>10</sub></sub>	624	764	1388	10
$10^2$	14513	DICCG <sub>POD<sub>5</sub></sub>	624	919	1543	11
$10^3$	12714	DICCG <sub>POD<sub>10</sub></sub>	524	700	1224	10
$10^3$	12714	DICCG <sub>POD<sub>5</sub></sub>	524	923	1447	11
$10^4$	11151	DICCG <sub>POD<sub>10</sub></sub>	482	783	1265	11
$10^4$	11151	DICCG <sub>POD<sub>5</sub></sub>	482	960	1442	13
$10^5$	10958	DICCG <sub>POD<sub>10</sub></sub>	469	982	1451	13
$10^5$	10958	DICCG <sub>POD<sub>5</sub></sub>	469	1078	1547	14
$10^6$	9735	DICCG <sub>POD<sub>10</sub></sub>	442	1163	1605	16
$10^6$	9735	DICCG <sub>POD<sub>5</sub></sub>	442	1317	1759	18

Table 4: Comparison between the ICCG and DICCG methods of the average number of linear iterations for various contrast between permeability layers. Injection through the left boundary, domain 32 x 32 cells.

We observe in Table 4 that when we use deflation methods, the number of linear iterations is reduced up to  $\approx 7\%$  of the total number of iterations computed with ICCG. In

this table, we also observe that the number of iterations does not change dramatically when we vary the contrast between permeability layers. However, we observe an increase when we have a contrast between permeability layers of  $10^6$ . Finally, we note that the results are similar for the two deflation approaches, 10 and 5 POD basis vectors as deflation vectors. In figure 6, we observe that the eigenvalues of the correlation matrix for a contrast on the permeability layers of  $10^1$  and  $10^6$  are similar. In both cases, we have four eigenvalues significantly larger than the rest of the eigenvalues. Therefore, if we use five POD vectors instead of ten as deflation vectors, the results are similar, which is shown in Table 4. For the case of higher contrast, the smallest eigenvalues are slightly smaller than with smaller contrast. Therefore, the results are slightly better for the case with smaller contrast. In Figure , we observe that the pressure is larger on the boundary where water is injected and it decreases as we get close to the opposite boundary. We also observe that the water flows easily through the layers with higher permeability (see Figure 5).

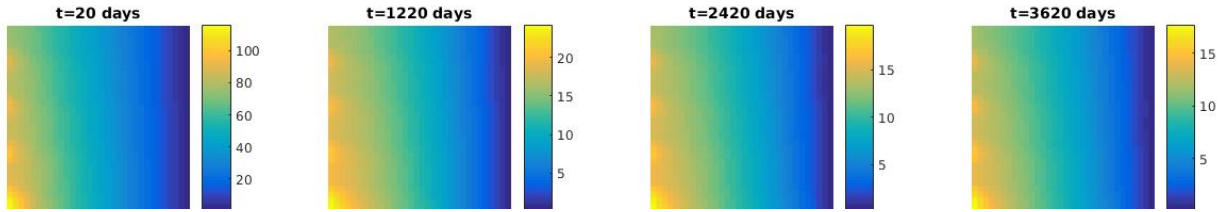


Figure 4: Pressure field [bars] for various times, for a contrast between permeability values of  $10^1$ ,  $32 \times 32$  grid cells.

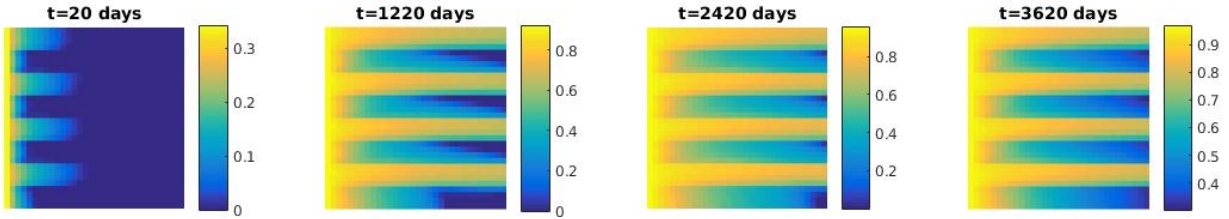


Figure 5: Water saturation for various times, for a contrast between permeability values of  $10^1$ ,  $32 \times 32$  grid cells.

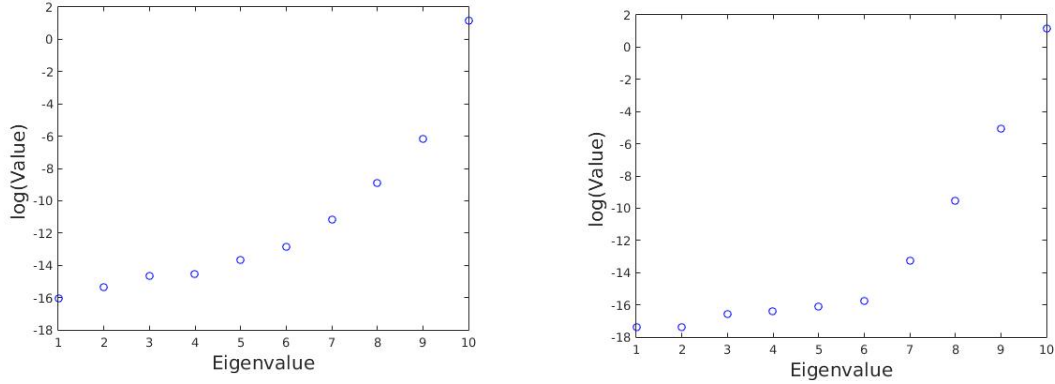


Figure 6: Eigenvalues of the correlation matrix  $\mathbf{R} = \frac{1}{m}\mathbf{X}\mathbf{X}^T$  for a contrast between permeability values of  $10^1$  and  $10^6$ .

### A: Injection through the left boundary, capillary pressure included.

For this set of experiments, we include capillary pressure. The capillary pressure function used for these experiments is presented in Table 1 and Figure 3. In Table 5, the number of iterations necessary to achieve convergence is presented for various contrast between permeability layers for the ICCG and DICCG methods, the latter with different selection of POD basis vectors as deflation vectors. The pressure field and the water saturation are presented in Figure 7 and Figure 8 for various times.

In Table 5, we observe that the behavior of the DICCG method is similar when we use 5 or 10 POD basis vectors as deflation vectors (see Figure 9). We observe that the performance of the DICCG method is not as good as without capillary pressure. However, we observe that for a contrast between permeability layers less than  $10^4$  we need around 20% of the number of ICCG iterations. For a larger contrast, we need between 30 to 40% of the ICCG number of iterations.

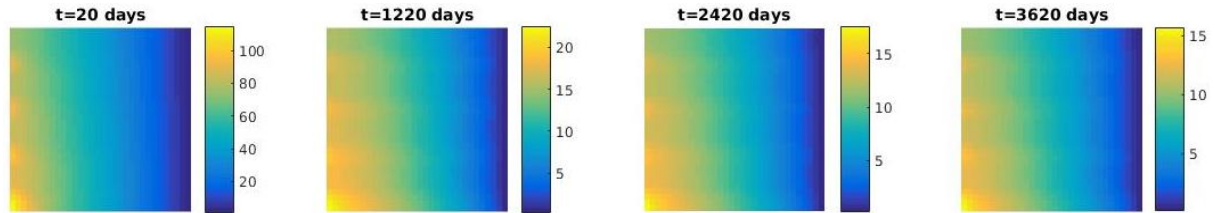


Figure 7: Pressure field [bars] for various times for a contrast between permeability values of  $10^1$ ,  $32 \times 32$  grid cells.

We note, in Figure 9, that the eigenvalues of the correlation matrix are more spread when the contrast between permeability layers is  $10^6$ . While the maximum is similar for both cases, the minimum for a contrast of  $10^1$  is around  $-14$  and for a contrast of  $10^6$  is around  $-16$ , which is two orders of magnitude difference. The latter can hamper the behavior of the DICCG method for larger contrast. However, we also note that the largest



$\frac{\sigma_2}{\sigma_1}$	Total ICCG	Method	ICCG Snapshots	DICCG	Total ICCG +DICCG	% of total ICCG
$10^0$	12440	DICCG <sub>POD<sub>10</sub></sub>	500	2050	2550	20
$10^0$	12440	DICCG <sub>POD<sub>5</sub></sub>	500	1951	2451	20
$10^1$	14597	DICCG <sub>POD<sub>10</sub></sub>	600	2843	3443	24
$10^1$	14597	DICCG <sub>POD<sub>5</sub></sub>	600	3072	3672	25
$10^2$	14897	DICCG <sub>POD<sub>10</sub></sub>	618	2517	3135	21
$10^2$	14897	DICCG <sub>POD<sub>5</sub></sub>	618	2588	3206	22
$10^3$	11821	DICCG <sub>POD<sub>10</sub></sub>	502	2439	2941	25
$10^3$	11821	DICCG <sub>POD<sub>5</sub></sub>	502	2362	2864	24
$10^4$	10530	DICCG <sub>POD<sub>10</sub></sub>	465	2491	2956	28
$10^4$	10530	DICCG <sub>POD<sub>5</sub></sub>	465	2464	2929	28
$10^5$	10030	DICCG <sub>POD<sub>10</sub></sub>	451	2952	3403	34
$10^5$	10030	DICCG <sub>POD<sub>5</sub></sub>	451	2770	3221	32
$10^6$	9071	DICCG <sub>POD<sub>10</sub></sub>	428	3156	3584	40
$10^6$	9071	DICCG <sub>POD<sub>5</sub></sub>	428	2644	3072	34

Table 5: Comparison between the ICCG and DICCG methods of the average number of linear iterations for various contrast between permeability layers. Injection through the left boundary, domain 32 x 32 cells, capillary pressure included.

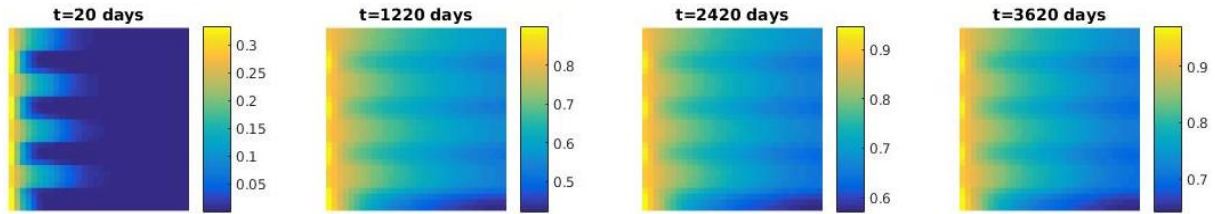


Figure 8: Water saturation for various times for a contrast between permeability values of  $10^1$ , 32 x 32 grid cells.

five eigenvalues are similar for both cases.

To further investigate the performance of the DICCG method in this case, we study three cases. In the first one, we increase the number of deflation vectors to 20. For the second one, we use a smaller time step (half of the previous) and we use 10 deflation vectors. For the last case, we use 20 deflation vectors and the same time step as in the second case.

#### Case 1

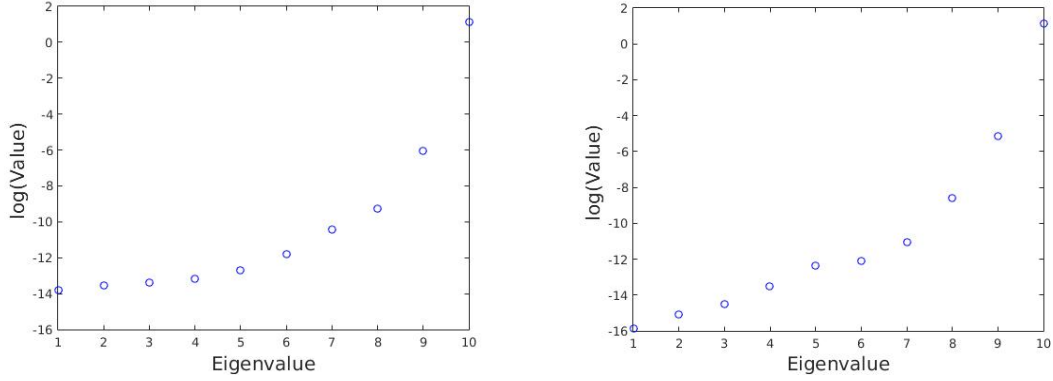


Figure 9: Eigenvalues of the correlation matrix  $\mathbf{R} = \frac{1}{m}\mathbf{X}\mathbf{X}^T$  for a contrast between permeability values of  $10^1$  and  $10^6$ , capillary pressure included.

$\frac{\sigma_2}{\sigma_1}$	Total ICCG	Method	ICCG Snapshots	DICCG	Total ICCG +DICCG	% of total ICCG
$10^0$	12440	DICCG <sub>POD<sub>20</sub></sub>	1010	1815	2825	23
$10^0$	12440	DICCG <sub>POD<sub>11</sub></sub>	1010	1497	2507	20
$10^1$	14597	DICCG <sub>POD<sub>20</sub></sub>	1210	2347	3557	24
$10^1$	14597	DICCG <sub>POD<sub>11</sub></sub>	1210	2486	3696	25
$10^2$	14897	DICCG <sub>POD<sub>20</sub></sub>	1248	2136	3384	23
$10^2$	14897	DICCG <sub>POD<sub>11</sub></sub>	1248	2233	3481	23
$10^3$	11821	DICCG <sub>POD<sub>20</sub></sub>	1002	2082	3084	26
$10^3$	11821	DICCG <sub>POD<sub>11</sub></sub>	1002	2170	3172	27
$10^4$	10530	DICCG <sub>POD<sub>20</sub></sub>	954	2272	3226	31
$10^4$	10530	DICCG <sub>POD<sub>11</sub></sub>	954	2312	3266	31
$10^5$	10030	DICCG <sub>POD<sub>20</sub></sub>	928	2761	3689	37
$10^5$	10030	DICCG <sub>POD<sub>11</sub></sub>	928	2875	3803	38
$10^6$	9071	DICCG <sub>POD<sub>20</sub></sub>	837	3229	4066	45
$10^6$	9071	DICCG <sub>POD<sub>11</sub></sub>	837	2927	3764	41

Table 6: Comparison between the ICCG and DICCG methods of the average number of linear iterations for various contrast between permeability layers. Injection through the left boundary, domain 32 x 32 cells, capillary pressure included, 20 deflation vectors.

We observe in Figure 10 that the range of the spectrum of the correlation matrix is similar to the case when we have 10 deflation vectors. Therefore, the behavior of the DICCG method with 10 and 20 deflation vectors is similar (see Table 6).

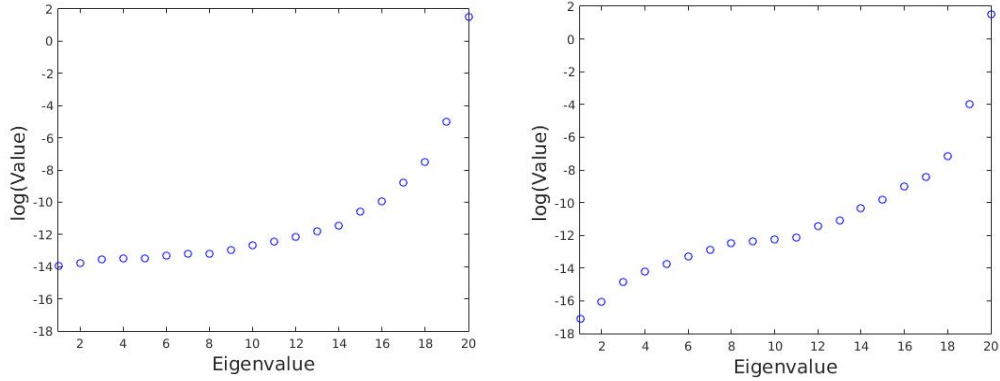


Figure 10: Eigenvalues of the correlation matrix  $\mathbf{C} = \mathbf{X}^T \mathbf{X}$  for a contrast between permeability values of  $10^1$  and  $10^6$ , capillary pressure included, 20 deflation vectors.

## Case 2

For this case, we use 480 time steps, instead of the 240 of the previous cases. In Table 7 we present the number of iterations of the ICCG and DICCG methods. We observe that the DICCG method performs better if we have smaller time step. In Figure 11, we observe note that the smallest eigenvalue is 10 – 15 for a contrast of  $10^1$  and 10 – 17 for a contrast of  $10^6$ . Therefore, the difference between these values is the same as in the previous cases, but the smallest value is smaller, which leads to a better performance.

$\frac{\sigma_2}{\sigma_1}$	Total ICCG	Method	ICCG Snapshots	DICCG	Total ICCG +DICCG	% of total ICCG
$10^0$	24882	DICCG <sub>POD<sub>10</sub></sub>	495	3362	3857	16
$10^0$	24882	DICCG <sub>POD<sub>5</sub></sub>	495	3324	3819	15
$10^1$	29187	DICCG <sub>POD<sub>10</sub></sub>	585	4166	4751	16
$10^1$	29187	DICCG <sub>POD<sub>5</sub></sub>	585	4463	5048	17
$10^2$	29795	DICCG <sub>POD<sub>10</sub></sub>	617	3598	4215	14
$10^2$	29795	DICCG <sub>POD<sub>5</sub></sub>	617	3777	4394	15
$10^3$	23617	DICCG <sub>POD<sub>10</sub></sub>	513	3434	3947	17
$10^3$	23617	DICCG <sub>POD<sub>5</sub></sub>	513	3445	3958	17
$10^5$	20047	DICCG <sub>POD<sub>10</sub></sub>	413	4230	4643	23
$10^5$	20047	DICCG <sub>POD<sub>5</sub></sub>	413	4000	4413	22
$10^6$	18400	DICCG <sub>POD<sub>10</sub></sub>	393	4623	5016	27
$10^6$	18400	DICCG <sub>POD<sub>5</sub></sub>	393	4005	4398	24

Table 7: Comparison between the ICCG and DICCG methods of the average number of linear iterations for various contrast between permeability layers. Injection through the left boundary, domain 32 x 32 cells, capillary pressure included (480 time steps).

From these experiments, we observe that the performance of the DICCG method depends on the time step. This can be linked to the information acquired with the snapshots.

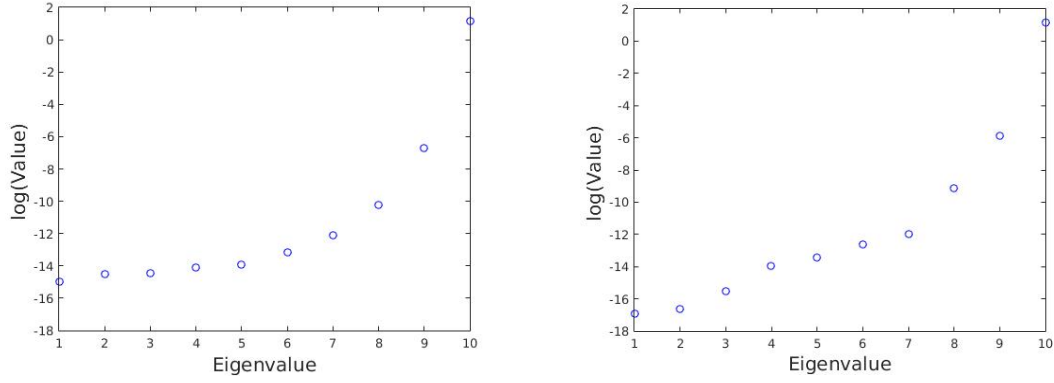


Figure 11: Eigenvalues of the correlation matrix  $\mathbf{C} = \mathbf{X}^T \mathbf{X}$  for a contrast between permeability values of  $10^1$  and  $10^6$ , 480 time steps.

For the case without capillary pressure, the time step used is enough to capture the system behavior. On the contrary, for the case when we have capillary pressure involved, it is necessary to take into account smaller changes produced in the system, which can be done by taking smaller time steps.

## B: Injection through the left boundary, no capillary pressure, gravity included (3D).

In this section, we repeat the experiments performed in the 2D case for a 3D problem with  $24 \times 24 \times 24$  cells. As in the previous case, each cell is one meter long. We studied two layered problems. In the first one, the layers are placed vertically (see Figure 12) and in the second, an horizontal configuration is used (see Figure 13). In Tables 8 and 9, the number of iterations necessary to achieve convergence are presented for various contrast between permeability layers for the ICCG and DICCG methods. The pressure field and the water saturation are presented in Figures 14 and 16 for various times for the first case, and Figures 18 and 19 for the second.

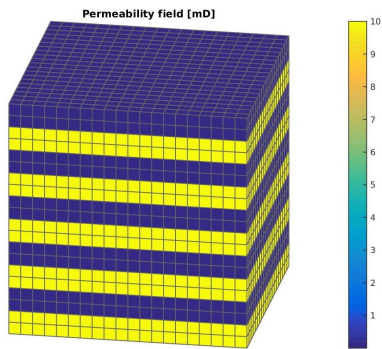


Figure 12: Rock permeability

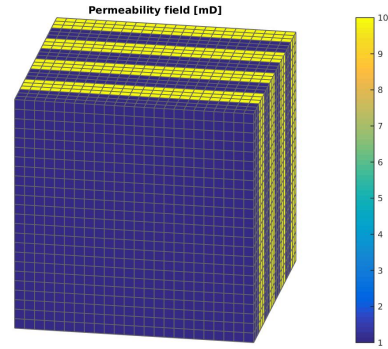


Figure 13: Rock permeability

$\frac{\sigma_2}{\sigma_1}$	Total ICCG	Method	ICCG Snapshots	DICCG	Total ICCG +DICCG	% of total ICCG
$10^0$	15438	DICCG <sub>POD<sub>10</sub></sub>	574	1616	2190	14
$10^0$	15438	DICCG <sub>POD<sub>5</sub></sub>	574	1871	2445	16
$10^1$	17496	DICCG <sub>POD<sub>10</sub></sub>	656	1800	2456	14
$10^1$	17496	DICCG <sub>POD<sub>5</sub></sub>	656	2170	2826	16
$10^2$	20587	DICCG <sub>POD<sub>10</sub></sub>	791	2023	2814	14
$10^2$	20587	DICCG <sub>POD<sub>5</sub></sub>	791	2251	3042	15
$10^3$	20044	DICCG <sub>POD<sub>10</sub></sub>	602	1888	2490	12
$10^3$	20044	DICCG <sub>POD<sub>5</sub></sub>	602	2236	2838	14
$10^4$	17563	DICCG <sub>POD<sub>10</sub></sub>	530	1782	2312	13
$10^4$	17563	DICCG <sub>POD<sub>5</sub></sub>	530	2140	2670	15
$10^5$	16944	DICCG <sub>POD<sub>10</sub></sub>	513	1874	2387	14
$10^5$	16944	DICCG <sub>POD<sub>5</sub></sub>	513	2124	2637	16
$10^6$	15720	DICCG <sub>POD<sub>10</sub></sub>	486	1972	2458	16
$10^6$	15720	DICCG <sub>POD<sub>5</sub></sub>	486	2121	2607	17

Table 8: Comparison between the ICCG and DICCG methods of the average number of linear iterations for various contrast between permeability layers. Injection through the left boundary, domain 24 x 24 x 24 cells, no capillary pressure, gravity included.

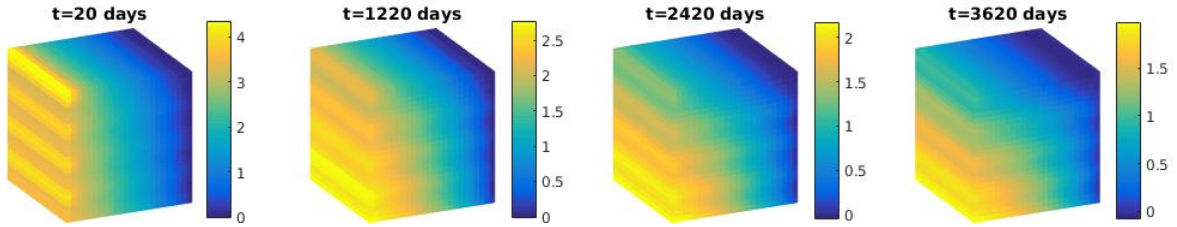


Figure 14: Pressure field for various times for a contrast between permeability values of  $10^1$ , 24 x 24 x 24 grid cells, horizontal layers.

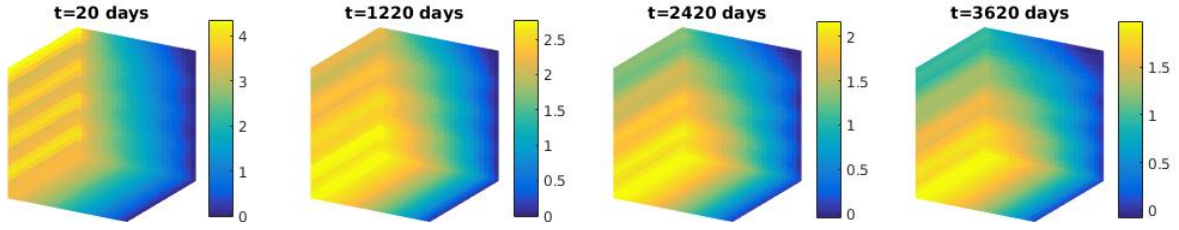


Figure 15: Pressure field for various times for a contrast between permeability values of  $10^1$ ,  $24 \times 24 \times 24$  grid cells, horizontal layers, lower view.

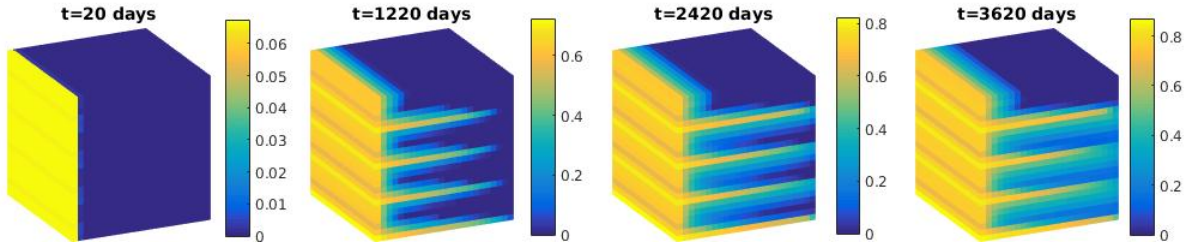


Figure 16: Water saturation for various times for a contrast between permeability values of  $10^1$ ,  $24 \times 24 \times 24$  grid cells, horizontal layers.

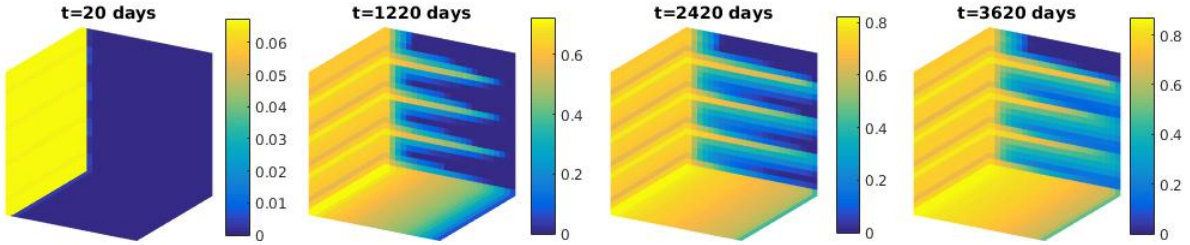


Figure 17: Water saturation for various times for a contrast between permeability values of  $10^1$ ,  $24 \times 24 \times 24$  grid cells, horizontal layers, lower view.

In Tables 8 and 9, we observe a reduction of around 15% of the number of ICCG iterations when we use DICCG. We note that the results are similar when we use ten or five deflation vectors. We can also note that the reduction does not depend on the contrast in permeability layers or the position of the layers.



$\frac{\sigma_2}{\sigma_1}$	Total ICCG	Method	ICCG Snapshots	DICCG	Total ICCG +DICCG	% of total ICCG
$10^0$	15438	DICCG <sub>POD<sub>10</sub></sub>	574	1616	2190	14
$10^0$	15438	DICCG <sub>POD<sub>5</sub></sub>	574	1871	2445	16
$10^1$	19426	DICCG <sub>POD<sub>10</sub></sub>	654	1969	2623	14
$10^1$	19426	DICCG <sub>POD<sub>5</sub></sub>	654	2258	2912	15
$10^2$	22577	DICCG <sub>POD<sub>10</sub></sub>	762	2340	3102	14
$10^2$	22577	DICCG <sub>POD<sub>5</sub></sub>	762	2714	3476	15
$10^3$	21832	DICCG <sub>POD<sub>10</sub></sub>	594	2086	2680	12
$10^3$	21832	DICCG <sub>POD<sub>5</sub></sub>	594	2406	3000	14
$10^4$	18483	DICCG <sub>POD<sub>10</sub></sub>	529	1868	2397	13
$10^4$	18483	DICCG <sub>POD<sub>5</sub></sub>	529	2121	2650	14
$10^5$	17808	DICCG <sub>POD<sub>10</sub></sub>	513	1819	2332	13
$10^5$	17808	DICCG <sub>POD<sub>5</sub></sub>	513	2065	2578	14
$10^6$	17152	DICCG <sub>POD<sub>10</sub></sub>	486	1955	2441	14
$10^6$	17152	DICCG <sub>POD<sub>5</sub></sub>	486	2115	2601	15

Table 9: Comparison between the ICCG and DICCG methods of the average number of linear iterations for various contrast between permeability layers. Injection through the left boundary, domain 24 x 24 x 24 cells, no capillary pressure, gravity included, vertical layers.

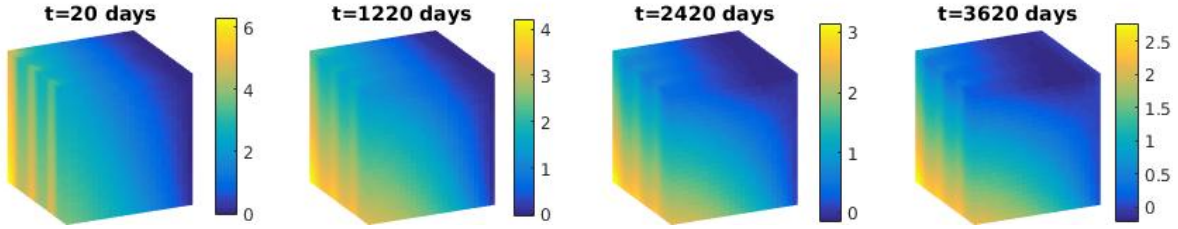


Figure 18: Pressure field for various times for a contrast between permeability values of  $10^1$ , 24 x 24 x 24 grid cells, vertical layers.

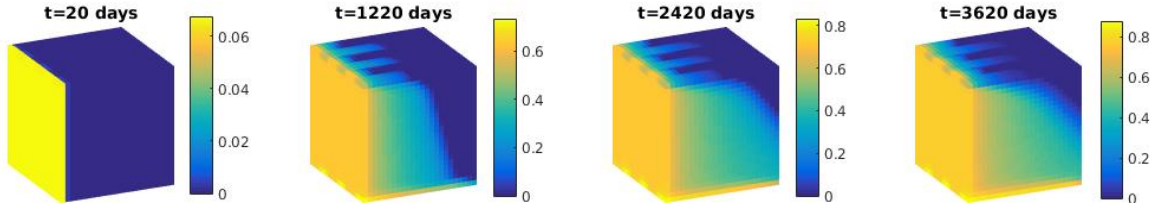


Figure 19: Water saturation for various times for a contrast between permeability values of  $10^1$ , 24 x 24 x 24 grid cells, vertical layers.



### C: Injection through the left boundary, capillary pressure and gravity included (3D).

As in the previous case, we study a 3D problem with gravity terms included, but in this case we also include capillary pressure. The capillary pressure function is the same as in the 2D problem (see Table 1 and Figure 3). The number of iterations necessary to achieve convergence are presented for various contrast between permeability layers for the ICCG and DICCG methods in Table 10 . The pressure field and the water saturation are presented in Figures 20 and 21 for various times.

$\frac{\sigma_2}{\sigma_1}$	Total ICCG	Method	ICCG Snapshots	DICCG	Total ICCG +DICCG	% of total ICCG
$10^0$	14136	DICCG <sub>POD<sub>10</sub></sub>	588	2357	2945	21
$10^0$	14136	DICCG <sub>POD<sub>5</sub></sub>	588	2520	3108	22
$10^1$	16614	DICCG <sub>POD<sub>10</sub></sub>	672	2786	3458	21
$10^1$	16614	DICCG <sub>POD<sub>5</sub></sub>	672	3130	3802	23
$10^2$	20037	DICCG <sub>POD<sub>10</sub></sub>	786	3290	4076	20
$10^2$	20037	DICCG <sub>POD<sub>5</sub></sub>	786	3773	4559	23
$10^3$	18640	DICCG <sub>POD<sub>10</sub></sub>	610	2918	3528	19
$10^3$	18640	DICCG <sub>POD<sub>5</sub></sub>	610	3265	3875	21
$10^4$	15437	DICCG <sub>POD<sub>10</sub></sub>	522	2712	3234	21
$10^4$	15437	DICCG <sub>POD<sub>5</sub></sub>	522	3107	3629	24
$10^5$	14371	DICCG <sub>POD<sub>10</sub></sub>	505	2899	3404	24
$10^5$	14371	DICCG <sub>POD<sub>5</sub></sub>	505	3273	3778	26
$10^6$	13176	DICCG <sub>POD<sub>10</sub></sub>	470	3361	3831	29
$10^6$	13176	DICCG <sub>POD<sub>5</sub></sub>	470	2940	3410	26

Table 10: Comparison between the ICCG and DICCG methods of the average number of linear iterations for various contrast between permeability layers. Injection through the left boundary, domain 24 x 24 x 24 cells, capillary pressure and gravity included.

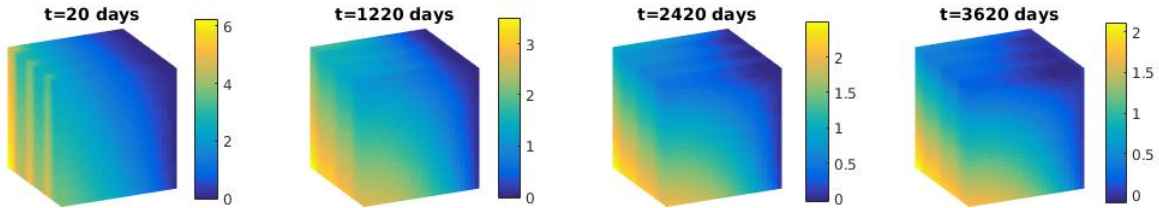


Figure 20: Pressure field for various times for a contrast between permeability values of  $10^1$ , 24 x 24 x 24 grid cells, capillary pressure and gravity included.

In Table 10, we observe that for the DICCG method we need around 20% of the number of iterations necessary for the ICCG. We also note that this percentage increases slightly

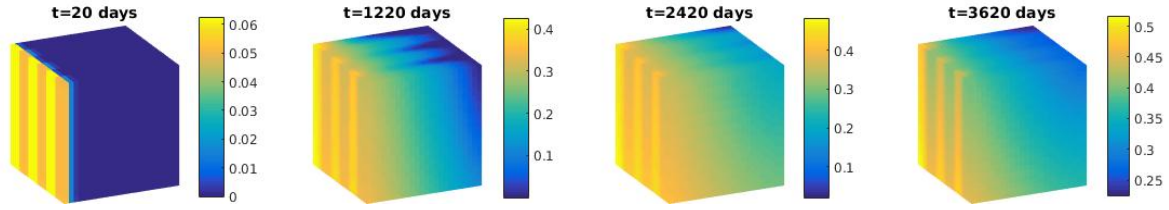


Figure 21: Water saturation for various times for a contrast between permeability values of  $10^1$ ,  $24 \times 24$  x 24 grid cells, capillary pressure and gravity included.

when we increase the contrast between permeability layers. If we compare with the case without capillary pressure, we observe that the performance is better without capillary pressure. As mentioned in the 2D case, this could be caused by the lack of information in the deflation vectors.

## Wells.

The experiments simulate flow through a porous medium with a constant porosity field of 0.25. For the first set of experiments, two wells are placed in the reservoir, for the second, five wells are placed. The pressure in the wells is presented for each experiment. On the boundaries, we imposed homogeneous Neumann boundary conditions (no flux). We study a problem with layered permeability values and the SPE 10 problem with different sizes. The characteristics of the fluids are presented in Table 1 and Figure 3. For the relative permeability of the fluids, the Corey model is used. The curves of this model are presented in Figure 2. No gravity terms and no capillary pressure are taken into account in the first set of experiments. In the second part of this section, we study 3D problem with gravity and capillary pressure included.

### Heterogeneous permeability layers, 2 wells, bhp controlled

In this section we study waterflooding with two wells. Water is injected in one well placed in a corner of the domain. The second well is placed in the opposite corner. The domain consist on 35 x 35 cells. It contains layers with different permeability (see Figure 22). The contrast between permeability layers varies from  $10^0$  to  $10^7$ . The pressure in the injector is 200 bars and in the producer is -200 bars (see Table 11). The fluid properties are the same as in the previous experiments (see Table 1 and Figure 3). As in the previous experiments, we study deflation method with five and ten POD basis vectors as deflation vectors. The number of iterations necessary to achieve convergence are presented in Table 12. The total time of the simulation is taken as the time when a volume of water corresponding to 1.2 of the pore volume of the reservoir, for an homogeneous problem, is injected. This total time is used for the rest of the simulations. We simulate 240 time steps. In Figures 23 and 29, the oil rate is presented for homogeneous problem and layers with a contrast of  $10^1$  and  $10^7$ . The water rate is presented in Figures 24, and 30 for the same experiments.

We observe, in Table 12, that the number of iterations needed to achieve convergence with the DICCG method is reduced up to  $\approx 25\%$  of the necessary ICCG iterations for the homogeneous problem. For the heterogeneous problem, the reduction achieved with DICCG is up to 5% of the ICCG iterations.

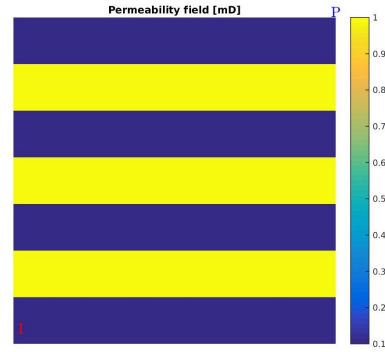


Figure 22: Rock permeability

Well	Water Sat	Oil Sat	Pressure
$I$	1	0	200 bars
$P$	0	1	-200 bars

Table 11: Wells properties.

$\frac{\sigma_2}{\sigma_1}$	Total ICCG	Method	ICCG Snapshots	DICCG	Total ICCG	% of total ICCG
$10^0$	9220	DICCG <sub>POD<sub>10</sub></sub>	389	1833	2222	24
$10^0$	9220	DICCG <sub>POD<sub>5</sub></sub>	389	2333	2722	30
$10^1$	14067	DICCG <sub>POD<sub>10</sub></sub>	590	1235	1825	13
$10^1$	14067	DICCG <sub>POD<sub>5</sub></sub>	590	1688	2278	16
$10^2$	16213	DICCG <sub>POD<sub>10</sub></sub>	670	787	1457	9
$10^2$	16213	DICCG <sub>POD<sub>5</sub></sub>	670	1107	1777	11
$10^3$	17379	DICCG <sub>POD<sub>10</sub></sub>	720	321	1041	6
$10^3$	17379	DICCG <sub>POD<sub>5</sub></sub>	720	449	1169	7
$10^4$	18334	DICCG <sub>POD<sub>10</sub></sub>	760	233	993	5
$10^4$	18334	DICCG <sub>POD<sub>5</sub></sub>	760	241	1001	5
$10^5$	19680	DICCG <sub>POD<sub>10</sub></sub>	820	233	1053	5
$10^5$	19680	DICCG <sub>POD<sub>5</sub></sub>	820	230	1050	5
$10^6$	20640	DICCG <sub>POD<sub>10</sub></sub>	860	234	1094	5
$10^6$	20640	DICCG <sub>POD<sub>5</sub></sub>	860	239	1099	5
$10^7$	16080	DICCG <sub>POD<sub>10</sub></sub>	670	513	1183	7
$10^7$	16080	DICCG <sub>POD<sub>5</sub></sub>	670	267	937	6

Table 12: Comparison between the ICCG and DICCG methods of the average number of linear iterations for the second NR iteration for various contrast between permeability layers.

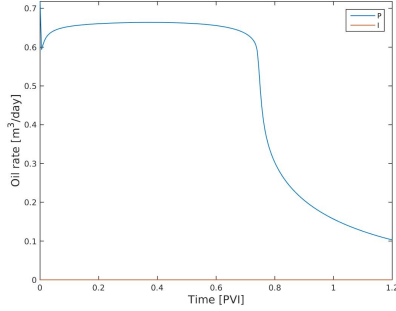


Figure 23: Oil Rate, homogeneous problem.

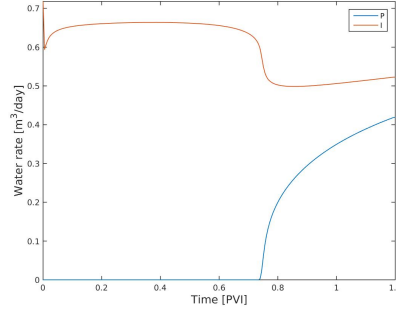


Figure 24: Water Rate, homogeneous problem.

We observe that, as the contrast in permeability increases, the injection rate of water decreases in around one order of magnitude when the contrast in permeability changes in one order of magnitude.

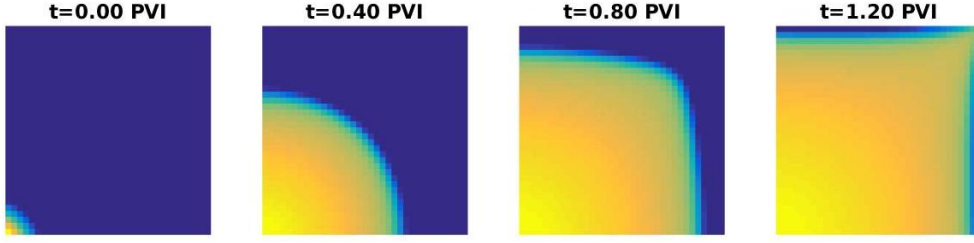


Figure 25: Water saturation, homogeneous problem.

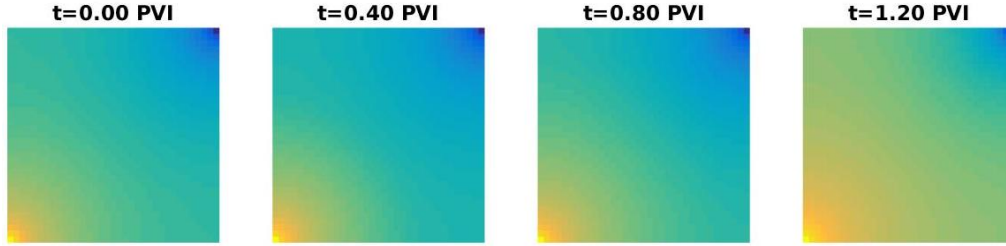


Figure 26: Pressure field, homogeneous problem.

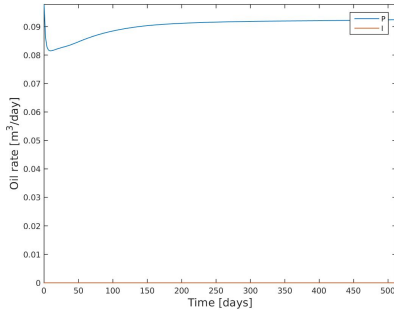


Figure 27: Oil Rate, contrast between permeability layers of  $10^1$ .

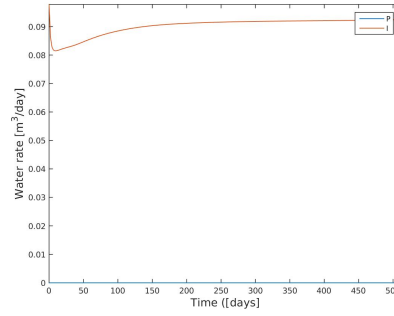


Figure 28: Water Rate, contrast between permeability layers of  $10^1$ .

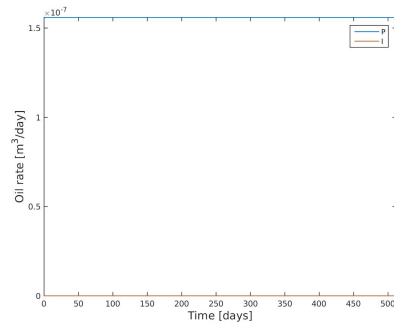


Figure 29: Oil Rate, contrast between permeability layers of  $10^7$ .

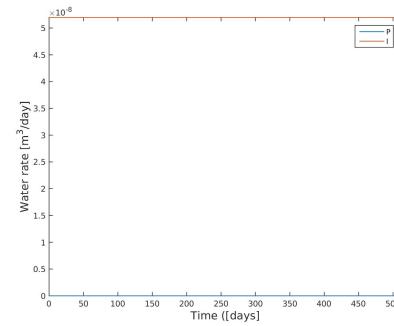


Figure 30: Water Rate, contrast between permeability layers of  $10^7$ .

## Five wells, bhp

### Heterogeneous permeability layers

For the first set of experiments, we study a layered system (see Figure 1). We use 6 layers of the same size, 3 layers with one value of permeability  $\sigma_1$ , followed by a layer with a different permeability value  $\sigma_2$ . The permeability of one set of layers is set to  $\sigma_1 = 100mD$ , the permeability of the other set  $\sigma_2$  is varied. Therefore, the contrast in permeability between the layers ( $\frac{\sigma_2}{\sigma_1} = \sigma_2$ ), depends on the value of  $\sigma_2$ . The permeability  $\sigma_2$  varies from  $\sigma_2 = 100mD$  to  $\sigma_2 = 10^{-3}mD$ . The domain consists of a Cartesian grid of 30 x 30 cells with a length of ten meters each cell.

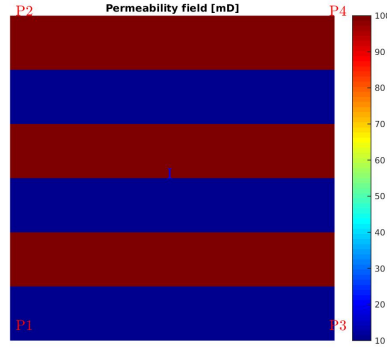


Figure 31: Rock permeability

One injector is placed in the center and four on the corners of the reservoir (see Figure 31). The wells are controlled via the bottom hole pressure (bhp). Water is injected into a reservoir initially filled with oil. The values of the wells are presented in Table 13. The first simulation has constant permeability through all the reservoir. The simulation is run until we inject 1.2 times the pore volume of the reservoir, this process takes 345 days. We used this time, as the total time of the rest of the experiments. We use 200 time steps.

Well	Water Sat	Oil Sat	Pressure
$P_1$	0	1	50 bars
$P_2$	0	1	50 bars
$P_3$	0	1	50 bars
$P_4$	0	1	50 bars
$I$	1	0	200 bars

Table 13: Wells properties.

Property	Value
$T_{total}$	1.2 PV
$T_{steps}$	1.2/200 PV

Table 14: Initial values of the system.

The number of iterations necessary to achieve convergence are presented in Table 15.

$\frac{\sigma_2}{\sigma_1}$	Total ICG	Method	ICCG Snapshots	DICCG	Total ICG + DICCG	% of total ICG
$10^0$	5445	DICCG <sub>POD<sub>10</sub></sub>	280	632	912	17
$10^0$	5445	DICCG <sub>POD<sub>5</sub></sub>	280	767	1047	19
$10^1$	8031	DICCG <sub>POD<sub>10</sub></sub>	400	781	1181	15
$10^1$	8031	DICCG <sub>POD<sub>5</sub></sub>	400	1011	1411	18
$10^2$	9788	DICCG <sub>POD<sub>10</sub></sub>	483	210	693	7
$10^2$	9788	DICCG <sub>POD<sub>5</sub></sub>	483	274	757	8
$10^3$	10779	DICCG <sub>POD<sub>10</sub></sub>	531	437	968	9
$10^3$	10779	DICCG <sub>POD<sub>5</sub></sub>	531	484	1015	9

Table 15: Comparison between the ICCG and DICCG methods.

### *Homogeneous permeability*

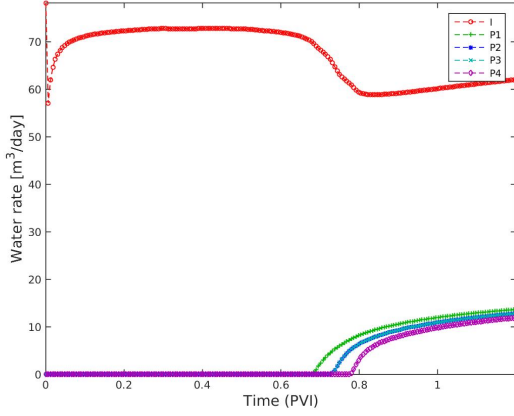


Figure 32: Water Rate, homogeneous permeability.

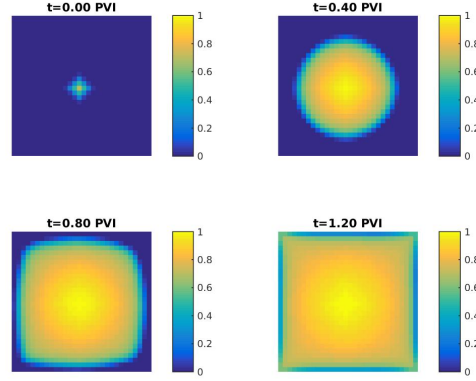


Figure 33: Water Saturation, homogeneous permeability.

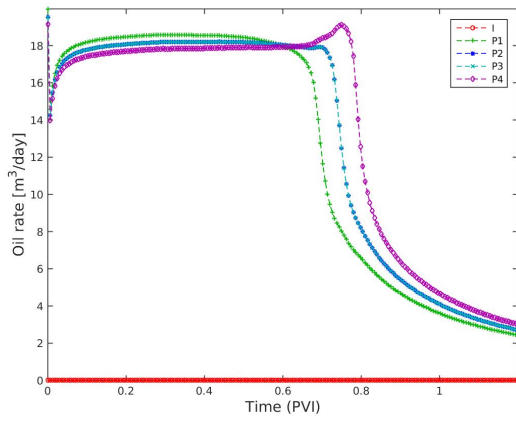


Figure 34: Oil rate, homogeneous permeability.

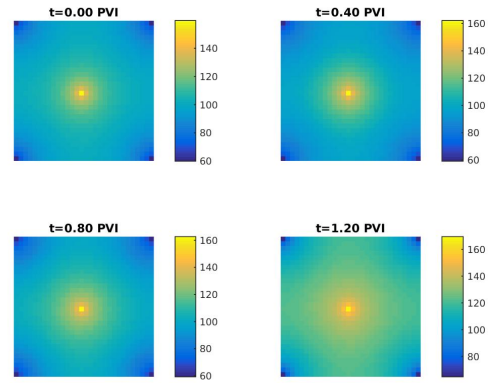


Figure 35: Pressure, homogeneous permeability.

### *Results heterogeneous permeability (contrast $10^1$ )*

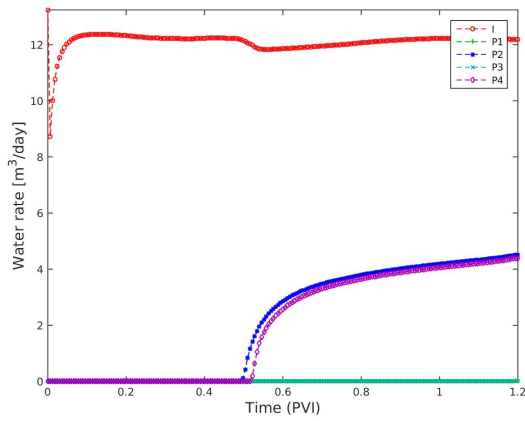


Figure 36: Water Rate, heterogeneous permeability (contrast  $10^1$ ).

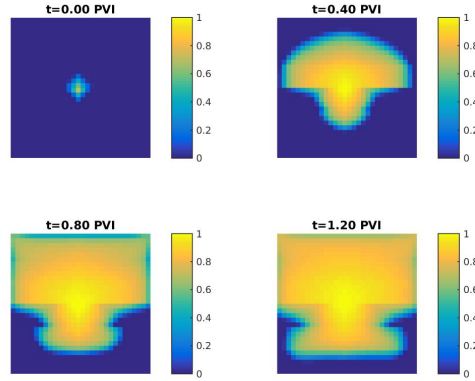


Figure 37: Water Saturation, heterogeneous permeability (contrast  $10^1$ ).



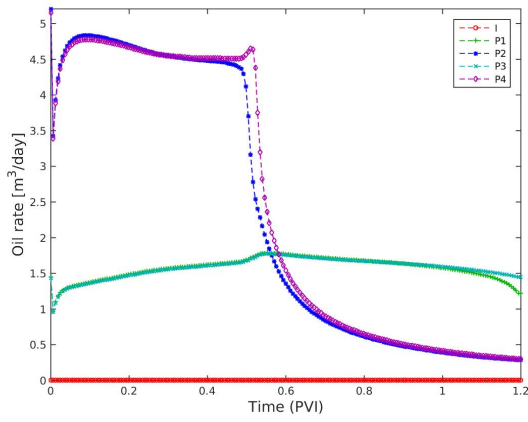


Figure 38: Oil rate, heterogeneous permeability (contrast  $10^1$ ).

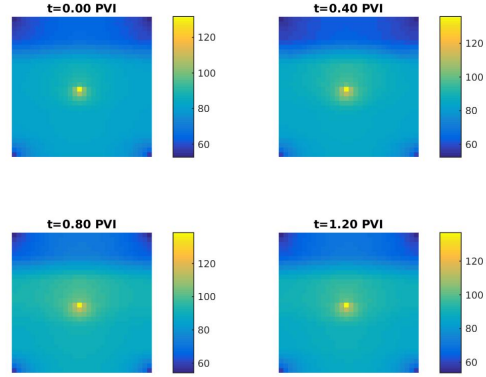


Figure 39: Pressure, heterogeneous permeability (contrast  $10^1$ ).

### *Results heterogeneous permeability (contrast $10^3$ )*

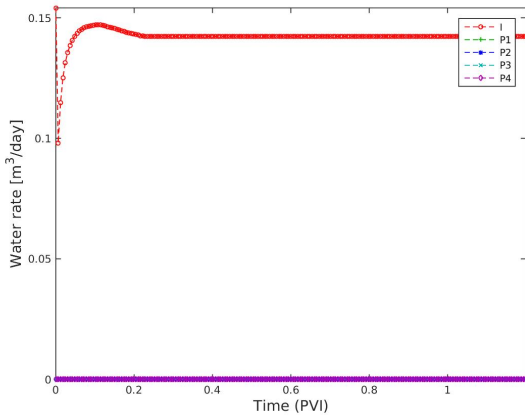


Figure 40: Water Rate, heterogeneous permeability (contrast  $10^3$ ).

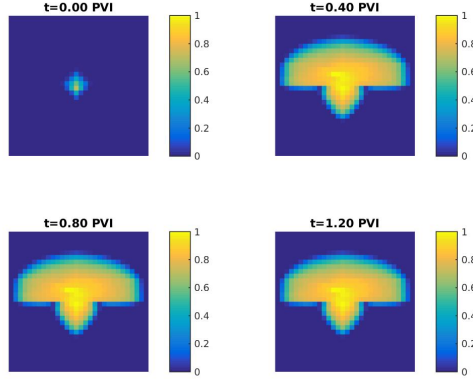


Figure 41: Water Saturation, heterogeneous permeability (contrast  $10^3$ ).

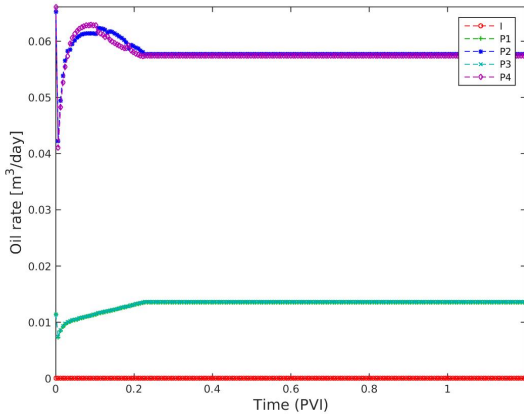


Figure 42: Oil rate, heterogeneous permeability (contrast  $10^3$ ).

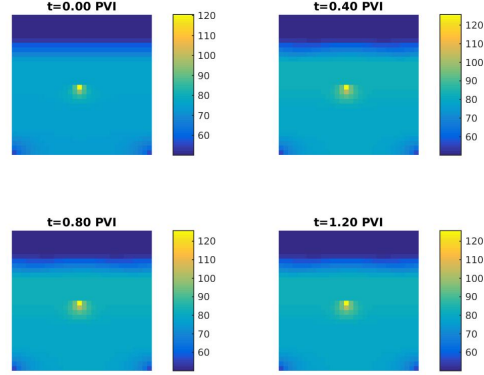


Figure 43: Pressure, heterogeneous permeability (contrast  $10^3$ ).

## 2.2 SPE 10

We study the SPE 10 model with 5 wells, 4 producers and one injector (see Figure ??). The original model contains  $60 \times 220 \times 85$  cells, in these experiments the grid sized is  $16 \times 56 \times 1$ . Only one layer is studied. The permeability and porosity fields are upscaled averaging the value in each grid cell using the function *sampleFromBox* from MRST. The permeability contrast for this problem is  $1.05 \times 10^7$ .

Well	Water Sat	Oil Sat	Pressure
$P_1$	0	1	275 bars
$P_2$	0	1	275 bars
$P_3$	0	1	275 bars
$P_4$	0	1	275 bars
$I$	1	0	1100 bars

Table 16: Wells properties.

Property	Value
$T_{total}$	1.2 PV
$T_{steps}$	1.2/200 PV

Table 17: Initial values of the system.

Total ICCG	Method	ICCG Snapshots	DICCG	Total ICCG + DICCG	% of total ICCG
11313	DICCG <sub>POD<sub>10</sub></sub>	567	1615	2182	19
11313	DICCG <sub>POD<sub>5</sub></sub>	567	2235	2802	25

Table 18: Comparison between the ICCG and DICCG methods of the average number of linear iterations for the SPE 10 problem,  $16 \times 56$  grid cells.

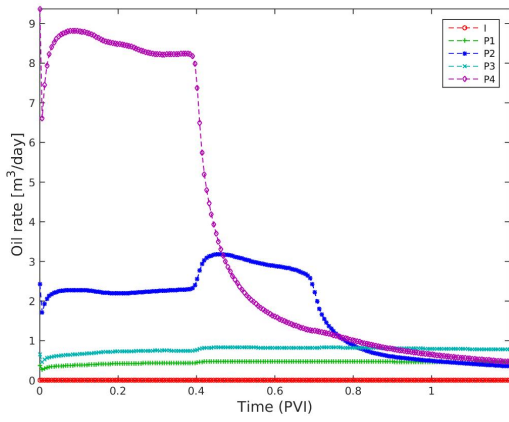


Figure 44: Oil rate, SPE 10, 16x56 grid cells.

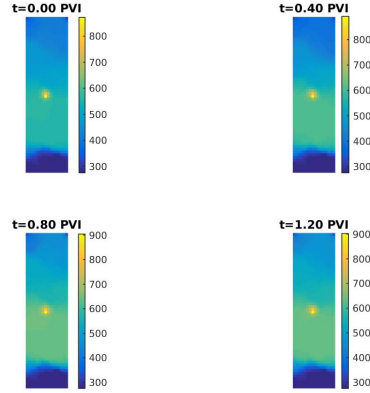


Figure 45: Pressure, SPE 10, 16x56 grid cells.

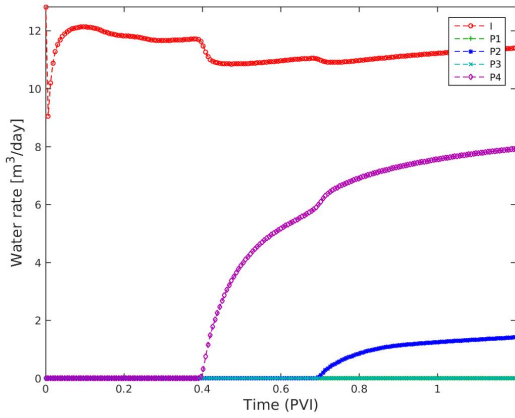


Figure 46: Water rate, SPE 10, 16x56 grid cells.

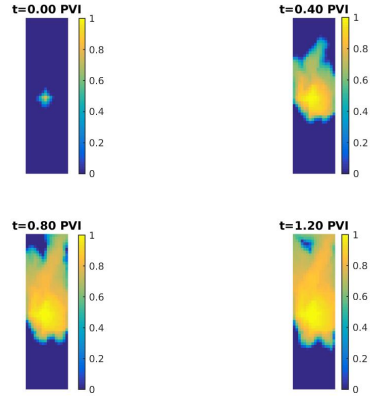


Figure 47: Water Saturation, SPE 10, 16x56 grid cells.

## 2.3 SPE 10, training simulation

We study the SPE 10 model with 5 wells, 4 producers and one injector (see Figure ??). The original model contains  $60 \times 220 \times 85$  cells, in these experiments the grid sized is  $16 \times 56 \times 1$ . Only one layer is studied. The permeability and porosity fields are upscaled averaging the value in each grid cell using the function *sampleFromBox* from MRST. The permeability contrast for this problem is  $1.05 \times 10^7$ .

Well	Water Sat	Oil Sat	Pressure
$P_1$	0	1	$rand(0 - 275)$ bars
$P_2$	0	1	$rand(0 - 275)$ bars
$P_3$	0	1	$275 - P_1$ bars
$P_4$	0	1	$275 - P_2$ bars
$I$	1	0	1100 bars

Table 19: Wells properties.

Property	Value
$T_{total}$	2 PV
$T_{steps}$	2/200 PV

Table 20: Initial values of the system.

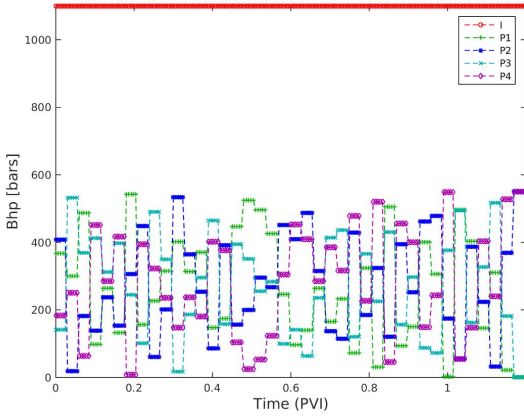


Figure 48: Bhp, SPE 10, 16x56 grid cells. training simulation.

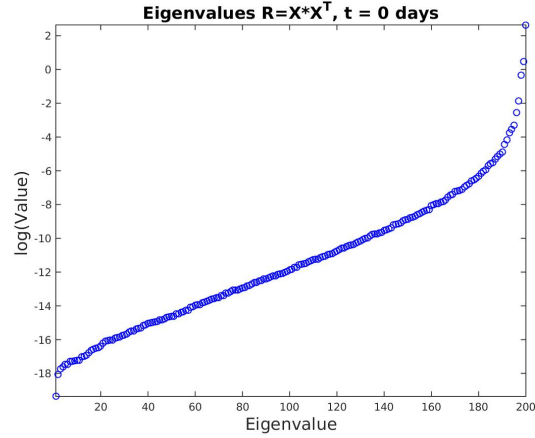


Figure 49: Eigenvalues training simulation, 200 timesteps.

SPE10

Well	Water Sat	Oil Sat	Pressure
$P_1$	0	1	275 bars
$P_2$	0	1	275 bars
$P_3$	0	1	275 bars
$P_4$	0	1	275 bars
$I$	1	0	1100 bars

Table 21: Wells properties.

Property	Value
$T_{total}$	1.2 PV
$T_{steps}$	1.2/200 PV

Table 22: Initial values of the system.

Total ICCG	Method	ICCG Snapshots	DICCG	Total ICCG + DICCG	% of total ICCG
11362	DICCG <sub>POD<sub>30</sub></sub>	106	1734	1840	16
11362	DICCG <sub>POD<sub>10</sub></sub>	151	2498	2649	23

Table 23: Comparison between the ICCG and DICCG methods of the average number of linear iterations for the SPE 10 problem, 16x56 grid cells.

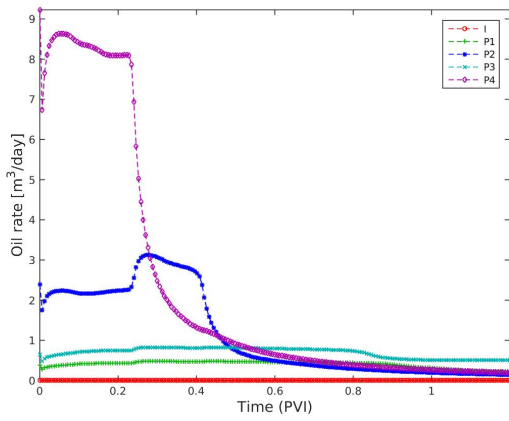


Figure 50: Oil rate, SPE 10, 16x56 grid cells.

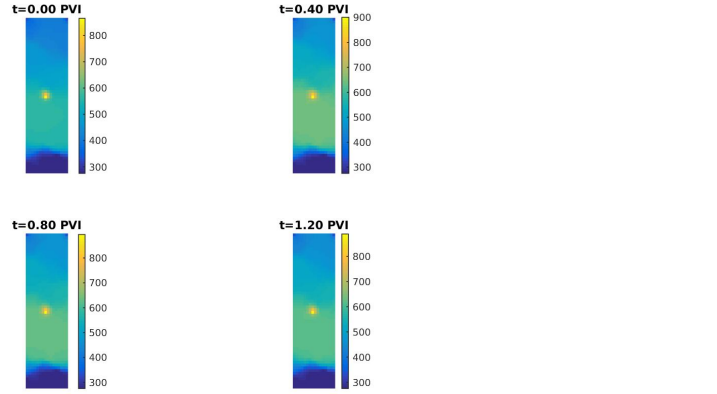


Figure 51: Pressure, SPE 10, 16x56 grid cells.

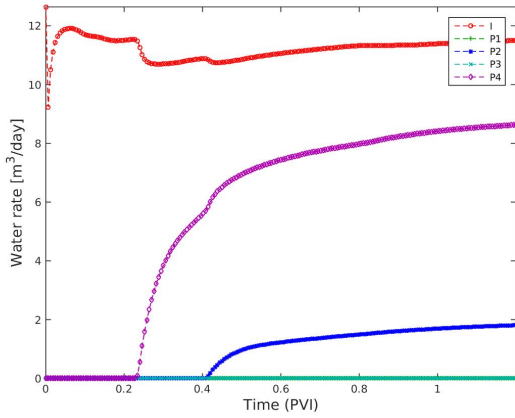


Figure 52: Water rate, SPE 10, 16x56 grid cells.

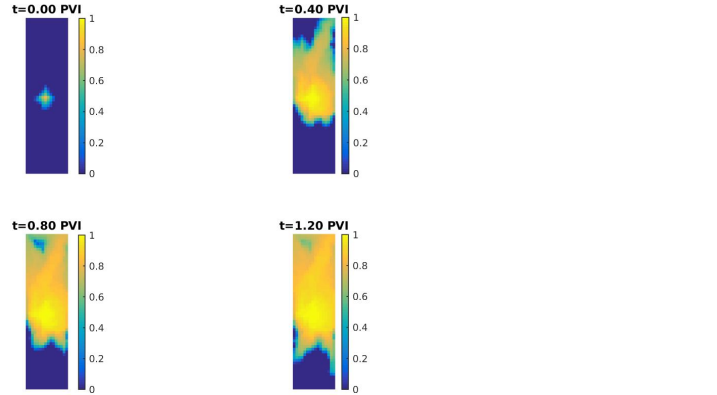


Figure 53: Water Saturation, SPE 10, 16x56 grid cells.

## Heterogeneous permeability layers, 2 wells, rate controlled

Layers with different permeability, 35 x 35 cells.

Well	Water Sat	Oil Sat	Pressure
$I$	0	1	$300m^3/day$
$P$	0	1	0 bars

Table 24: Wells properties.

$\frac{\sigma_2}{\sigma_1}$	Total ICCG	Method	ICCG Snapshots	DICCG	Total ICCG	% of total ICCG
$10^0$	37089	DICCG <sub>10</sub>	462	41878	42340	114
$10^0$	37089	DICCG <sub>POD10</sub>	462	31830	32292	87
$10^0$	37089	DICCG <sub>POD5</sub>	462	32355	32817	88

Table 25: Comparison between the ICCG and DICCG methods of the average number of linear iterations for the second NR iteration for various contrast between permeability layers.

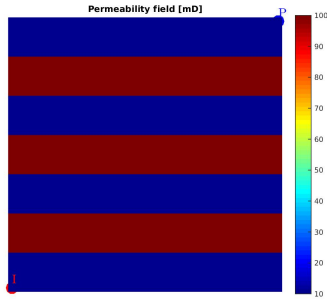


Figure 54: Rock perm.

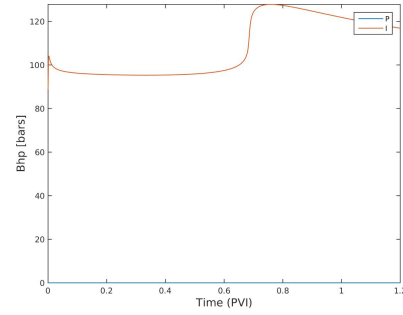


Figure 55: Bhp, homogeneous perm.

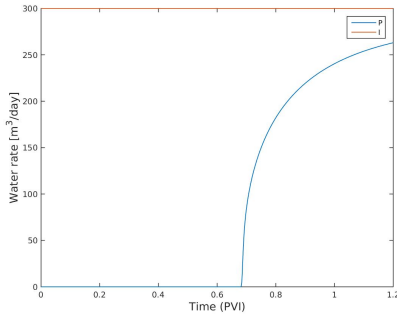


Figure 56: Water Rate.

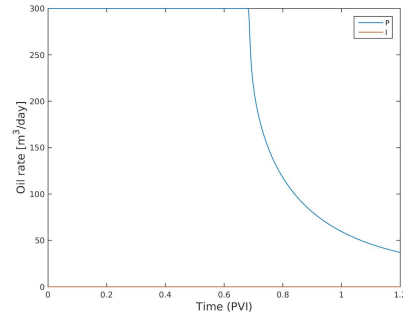


Figure 57: Oil rate.

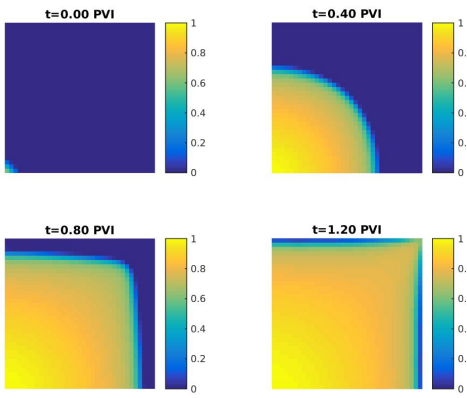


Figure 58: Water saturation.

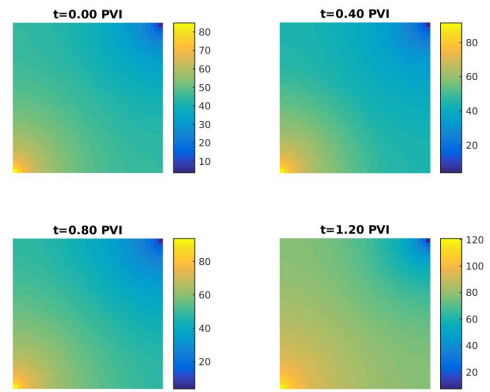


Figure 59: Pressure.

## References

- [1] K. Aziz and A. Settari. *Petroleum reservoir simulation*. Chapman & Hall, 1979.
- [2] Z. Chen, G. Huan and Y. Ma. *Computational methods for multiphase flows in porous media*. SIAM, 2006.
- [3] J.D. Jansen. *A systems description of flow through porous media*. Springer, 2013.
- [4] C. Vuik, A. Segal and J. A. Meijerink. An Efficient Preconditioned CG Method for the Solution of a Class of Layered Problems with Extreme Contrasts in the Coefficients. *Journal of Computational Physics*, 152:385, 1999.
- [5] J. Tang. *Two-Level Preconditioned Conjugate Gradient Methods with Applications to Bubbly Flow Problems*. PhD thesis, Delft University of Technology, 2008.
- [6] J.M. Tang, R. Nabben, C. Vuik and Y. Erlangga. Comparison of two-level preconditioners derived from deflation, domain decomposition and multigrid methods. *Journal of scientific computing*, 39(3):340–370, 2009.
- [7] M. Clemens, M. Wilke, R. Schuhmann and T. Weiland. Subspace projection extrapolation scheme for transient field simulations. *IEEE Transactions on Magnetics*, 40(2):934–937, 2004.
- [8] C. Vuik, A. Segal, L. Yaakoubi and E. Dufour. A comparison of various deflation vectors applied to elliptic problems with discontinuous coefficients. *Applied Numerical Mathematics*, 41(1):219–233, 2002.
- [9] B. Smith, P. Bjorstad and W. Gropp. *Domain decomposition: parallel multilevel methods for elliptic partial differential equations*. Cambridge University Press New York, 1996.
- [10] P. Astrid, G. Papaioannou, J.C. Vink and J.D. Jansen. Pressure Preconditioning Using Proper Orthogonal Decomposition. In *2011 SPE Reservoir Simulation Symposium, The Woodlands, Texas, USA*, January 2011.
- [11] R. Markovinović and J.D. Jansen. Accelerating iterative solution methods using reduced-order models as solution predictors. *International journal for numerical methods in engineering*, 68(5):525–541, 2006.
- [12] K.A. Lie. *An Introduction to Reservoir Simulation Using MATLAB: User guide for the Matlab Reservoir Simulation Toolbox (MRST)*. SINTEF ICT, 2013.
- [13] Y. Saad. *Iterative Methods for Sparse Linear Systems*. Society for Industrial and Applied Mathematics Philadelphia, PA, USA. 2nd edition, 2003.



## A ICCG

## B List of notation

Symbol	Quantity	Unit
$\phi$	Rock porosity	
$\mathbf{K}$	Rock permeability	<i>Darcy</i> ( $D$ )
$c_r$	Rock compressibility	$Pa^{-1}$
$\mathbf{v}$	Darcy's velocity	$m/d$
$\rho$	Fluid density	$kg/m^3$
$\mu$	Fluid viscosity	$Pa \cdot s$
$p$	Pressure	$Pa$
$g$	Gravity	$m/s^2$
$c_f$	Fluid compressibility	$Pa^{-1}$
$q$	Sources	

Table 26: Notation

## C Stopping criteria

When we use an iterative method, we always want that our approximation is close enough to the exact solution. In other words, we want that the error [13, pag. 42]:

$$\|\mathbf{e}^k\|_2 = \|\mathbf{x} - \mathbf{x}^k\|_2,$$

or the relative error:

$$\frac{\|\mathbf{x} - \mathbf{x}^k\|_2}{\|\mathbf{x}\|_2},$$

is small.

When we want to chose a stopping criteria, we could think that the relative error is a good candidate, but is has the disadvantage that we need to know the exact solution to compute it. What we have instead is the residual

$$\mathbf{r}^k = \mathbf{b} - \mathbf{A}\mathbf{x}^k,$$

that is actually computed in each iteration of the CG method. There is a relationship between the error and the residual that can help us with the choice of the stopping criteria.

$$\frac{\|\mathbf{x} - \mathbf{x}^k\|_2}{\|\mathbf{x}\|_2} \leq \kappa_2(A) \frac{\|\mathbf{r}^k\|_2}{\|\mathbf{b}\|_2}.$$

With this relationship in mind, we can choose the stopping criteria as an  $\epsilon$  for which

$$\frac{\|\mathbf{r}^k\|_2}{\|\mathbf{b}\|_2} \leq \epsilon.$$

But we should keep to have in mind the condition number of the matrix  $\mathbf{A}$ , because the relative error will be bounded by:

$$\frac{\|\mathbf{x} - \mathbf{x}^k\|_2}{\|\mathbf{x}\|_2} \leq \kappa_2(A)\epsilon.$$

## D Singular Value Decomposition for POD

If we perform SVD in  $\mathbf{X}$ , we have

$$\mathbf{X} = \mathbf{U}\Sigma\mathbf{V}^T, \quad \mathbf{U} \in \mathbb{R}^{n \times n}, \quad \Sigma \in \mathbb{R}^{n \times m}, \quad \mathbf{V} \in \mathbb{R}^{m \times m}.$$

Then we have

$$\begin{aligned} \mathbf{R} &= \mathbf{X}\mathbf{X}^T & \mathbf{R}^T &= \mathbf{X}^T\mathbf{X} \\ &= \mathbf{U}\Sigma\mathbf{V}^T(\mathbf{U}\Sigma\mathbf{V}^T)^T & &= (\mathbf{U}\Sigma\mathbf{V}^T)^T\mathbf{U}\Sigma\mathbf{V}^T \\ &= \mathbf{U}\Sigma\mathbf{V}^T\mathbf{V}\Sigma^T\mathbf{U}^T, \mathbf{V}^T\mathbf{V} = \mathbf{I} & &= \mathbf{V}\Sigma^T\mathbf{U}^T\mathbf{U}\Sigma\mathbf{V}^T, \mathbf{U}^T\mathbf{U} = \mathbf{I} \\ &= \mathbf{U}\Lambda\mathbf{U}^T, \Lambda = \Sigma\Sigma^T \in \mathbb{R}^{n \times n} & &= \mathbf{V}\Lambda^T\mathbf{V}^T, \Lambda^T = \Sigma^T\Sigma \in \mathbb{R}^{m \times m}. \end{aligned}$$

$$\mathbf{X} = \mathbf{U}\Sigma\mathbf{V}^T$$

$$\mathbf{U} = \mathbf{X}\mathbf{V}\Sigma^{-1}$$

$$\mathbf{U} = \mathbf{X}\mathbf{V}\Lambda^{-\frac{1}{2}}$$

If we compute  $\Lambda^T$ , we can compute  $\mathbf{U}$  as follows:

$$\mathbf{U} = \mathbf{X}\mathbf{V}(\Lambda^T)^{-\frac{T}{2}} = \mathbf{X}\mathbf{V}(\Lambda^T)^{\frac{1}{2}}$$

## E Deflation method

In this appendix, we explain how to obtain the solution of the linear system (??) with deflation. Some properties of the matrices used for deflation that will help us to find the solution of system (??) are [6]:

- a)  $\mathbf{P}^2 = \mathbf{P}$ .
- b)  $\mathbf{AP}^T = \mathbf{PA}$ .
- c)  $(\mathbf{I} - \mathbf{P}^T)\mathbf{x} = \mathbf{Qb}$ .
- d)  $\mathbf{PAQ} = \mathbf{0}^{n \times n}$ .
- e)  $\mathbf{PAZ} = \mathbf{0}^{n \times l}$ .

To obtain the solution of the linear system (??), we start with the splitting:

$$\mathbf{x} = \mathbf{x} - \mathbf{P}^T\mathbf{x} + \mathbf{P}^T\mathbf{x} = (\mathbf{I} - \mathbf{P}^T)\mathbf{x} + \mathbf{P}^T\mathbf{x}. \quad (33)$$

Multiplying expression (33) by  $\mathbf{A}$ , using the properties of the deflation matrices, we have:

$$\begin{aligned} \mathbf{Ax} &= \mathbf{A}(\mathbf{I} - \mathbf{P}^T)\mathbf{x} + \mathbf{AP}^T\mathbf{x}, & \text{Property :} \\ \mathbf{Ax} &= \mathbf{AQb} + \mathbf{AP}^T\mathbf{x}, & c) \\ \mathbf{b} &= \mathbf{AQb} + \mathbf{PAx}, & b), \end{aligned}$$

multiplying by  $\mathbf{P}$  and using the properties  $\mathbf{PAQ} = \mathbf{0}^{n \times n}$  and  $\mathbf{P}^2 = \mathbf{P}$ , properties d) and a), we have:

$$\begin{aligned} \mathbf{PAQb} + \mathbf{P}^2\mathbf{Ax} &= \mathbf{Pb}, \\ \mathbf{PAx} &= \mathbf{Pb}, \end{aligned}$$

where  $\mathbf{PAx} = \mathbf{Pb}$  is the deflated system. Since  $\mathbf{PA}$  is singular, the solution of Equation (34) can contain components of the null space of  $\mathbf{PA}$ ,  $(\mathcal{N}(\mathbf{PA}))$ . A solution of this system, called the deflated solution, is denoted by  $\hat{\mathbf{x}}$ . Then, the linear system to solve is:

$$\mathbf{PA}\hat{\mathbf{x}} = \mathbf{Pb}. \quad (34)$$

As the solution of Equation (34) can contain components of  $\mathcal{N}(\mathbf{PA})$ ,  $\hat{\mathbf{x}}$  can be decomposed as:

$$\hat{\mathbf{x}} = \mathbf{x} + \mathbf{y}, \quad (35)$$

with  $\mathbf{y} \in \mathcal{R}(\mathbf{Z}) \subset \mathcal{N}(\mathbf{PA})$ , and  $\mathbf{x}$  the solution of Equation (??).

Note: If  $\mathbf{y} \in \mathcal{R}(\mathbf{Z})$ , then

$$\mathbf{y} = \sum_{i=1}^m \alpha_i \mathbf{Z}_i,$$

$$\mathbf{PAy} = \mathbf{PA}(\mathbf{z}_1\alpha_1 + \dots + \mathbf{z}_m\alpha_m) = \mathbf{PAZ}\alpha,$$

from property e) we have:

$$\mathbf{PAy} = \mathbf{0}.$$

Therefore  $\mathcal{R}(\mathbf{Z}) \subset \mathcal{N}(\mathbf{PA})$ , and using property b) we have:

$$\mathbf{PAy} = \mathbf{AP}^T\mathbf{y} = \mathbf{0}.$$

As  $\mathbf{A}$  is invertible, we have:

$$\mathbf{P}^T\mathbf{y} = \mathbf{0}. \quad (36)$$

Multiplying Equation (35) by  $\mathbf{P}^T$  we obtain:

$$\mathbf{P}^T\hat{\mathbf{x}} = \mathbf{P}^T\mathbf{x} + \mathbf{P}^T\mathbf{y}.$$

substituting Equation (36) we arrive to:

$$\mathbf{P}^T\hat{\mathbf{x}} = \mathbf{P}^T\mathbf{x}. \quad (37)$$

Substitution of Equation (37) and property c) in Equation (33) leads to:

$$\mathbf{x} = \mathbf{Qb} + \mathbf{P}^T\hat{\mathbf{x}}, \quad (38)$$

which gives us the relation between  $\hat{\mathbf{x}}$  and  $\mathbf{x}$ .